Mode hopping in semiconductor lasers
by Timothy Alan Heumier

A thesis submitted in partial fulfillment of the requirements for the degree of Doctor of Philosophy in Physics
Montana State University

Abstract:
Semiconductor lasers have found widespread use in fiberoptic communications, merchandising (bar-code scanners), entertainment (videodisc and compact disc players), and in scientific inquiry (spectroscopy, laser cooling). Some uses require a minimum degree of stability of wavelength which is not met by these lasers: Under some conditions, semiconductor lasers can discontinuously switch wavelengths in a back-and-forth manner. This is called mode hopping.

We show that mode hopping is directly correlated to noise in the total intensity, and that this noise is easily detected by a photodiode. We also show that there are combinations of laser case temperature and injection current which lead to mode hopping. Conversely, there are other combinations for which the laser is stable. These results are shown to have implications for controlling mode hopping.

MODE HOPPING IN SEMICONDUCTOR LASERS

by

Timothy Alan Heumier

A thesis submitted in partial fulfillment
of the requirements for the degree

of

Doctor of Philosophy

in

Physics

MONTANA STATE UNIVERSITY
Bozeman, Montana

December, 1992

APPROVAL

of a thesis submitted by

Timothy Alan Heumier

This thesis has been read by each member of the thesis committee and has been found to be satisfactory regarding content, English usage, format, citations, bibliographical style, and consistency, and is ready for submission to the College of Graduate Studies.

12-4-92

Date

Chairperson, Graduate Committee

Approved for the Major Department

12-4-92

Date

Head, Major Department

Approved for the College of Graduate Studies

12/15/92

Date

Graduate Dean

STATEMENT OF PERMISSION TO USE

Signature Timothy A. Neuman

Date Dec. 7, 1992

ACKNOWLEDGEMENTS

It is my pleasure to acknowledge the persons who have helped me complete this endeavor. First and foremost, my thanks go to Almighty God in the person of Jesus the Christ, who made the wonderful Nature which I have studied so delightedly.

Further, I wish to thank my advisor, Dr. John L. Carlsten, for his great care and patience, gentle nudging and nurturing, and his boundless, infectious enthusiasm: Truly, it has been "fun".

I also wish to express gratitude to Eric Anderson, electronics whiz, and Norm Williams, machinist extraodinaire, for their patience and invaluable help in carrying out various aspects of this work.

In addition, several students helped immeasurably. Phil Battle, Jim Wessel, Rand Swanson, Meg Hall, Steve Sayhun, Andy Struckhoff, and undergraduates Heather Thomas and Ezra Szöke, and many others contributed in countless ways.

I gratefully acknowledge the support of ILX Lightwave, Inc.

To my wife, Annette, and my three children, Stacy, Josh and Holly, go the greatest praise. They supported me in so many ways: Financially, emotionally, spiritually. I know it was hard to put up with my prolonged absences, both physical and mental, and with the poverty of graduate school. To them go my utmost heartfelt thanks and love.

Tim Heumier, November, 1992

TABLE OF CONTENTS

LIST OF FIGURES

ABSTRACT

Semiconductor lasers have found widespread use in fiberoptic communications, merchandising (bar-code scanners), entertainment (videodisc and compact disc players), and in scientific inquiry (spectroscopy, laser cooling). Some uses require a minimum degree of stability of wavelength which is not met by these lasers: Under some conditions, semiconductor lasers can discontinuously switch wavelengths in a back-and-forth manner. This is called mode hopping.

We show that mode hopping is directly correlated to noise in the total intensity, and that this noise is easily detected by a photodiode. We also show that there are combinations of laser case temperature and injection current which lead to mode hopping. Conversely, there are other combinations for which the laser is stable. These results are shown to have implications for controlling mode hopping.

CHAPTER I

INTRODUCTION TO SEMICONDUCTOR LASERS

Uses for Semiconductor Lasers

Due to their small size, semiconductor lasers have many applications for which other lasers would be unsuited. They are found in compact disc and videodisc players, bar code scanners, optical communications and surveying. They are also used for studies of atomic structure [1]-[3] and quantum-mechanical effects [4].

Basic Characteristics of Semiconductor Lasers

A semiconductor laser is a very small device, about as large as a grain of salt (see Figure 1). Typical dimensions are 250 microns long, 100 microns wide, and around 100 microns thick. One type of laser in wide use is the GaAs/AlGaAs laser. It is comprised of a slab of (possibly doped) GaAs sandwiched between layers of AlGaAs which serve to confine the laser radiation. This is a crystalline structure which is cleaved in manufacture so that two opposite faces are smooth and parallel. These facets, whose power reflectivity is around 0.3, form the mirrors which provide the feedback for the gain needed for laser action.

The laser is pumped by an electrical current (called the injection current) which passes through the center slab (the active region) perpendicular to its plane. The current is usually confined to a narrow strip by some means, such as a current-blocking layer. As electrons are pumped from the valence band to the conduction band (see Figure 2), a population inversion is created. Lasing occurs when the electrons undergo stimulated emission and recombine with the holes left behind in the valence band. The laser beam, emitted from both facets equally, diverges strongly because of diffraction, since the light emerges from what amounts to a slit. The diffraction is therefore greatest perpendicular to the slit, giving rise to an elliptically-shaped beam, in contrast to the round beam so familiar in HeNe lasers and others. This highly divergent beam is almost always collimated by a short focal length lens such as a microscope objective.

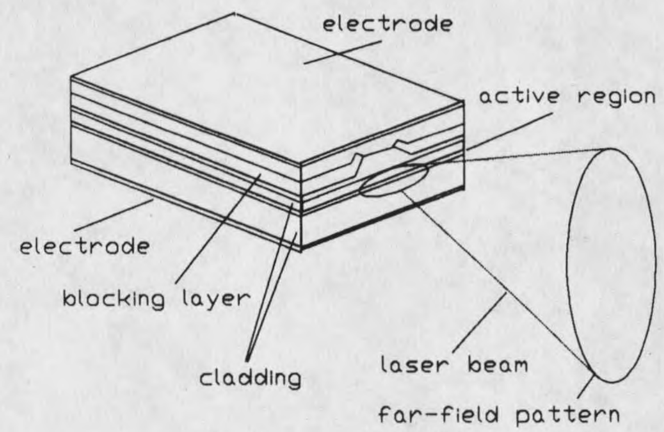

Figure 1. Schematic of typical laser diode chip. Cladding is GaAlAs, active region is GaAs. Blocking layer restricts current flow to narrow stripe through active region.

In the typical commercial semiconductor laser (or laser diode or diode laser, depending on the speaker), the crystal is mounted on a pedestal in a transistor-like package. The laser beam from the front facet exits through a glass window to the outside world. The beam from the other facet usually strikes a built-in photodiode which can be used to monitor the laser's optical power output.

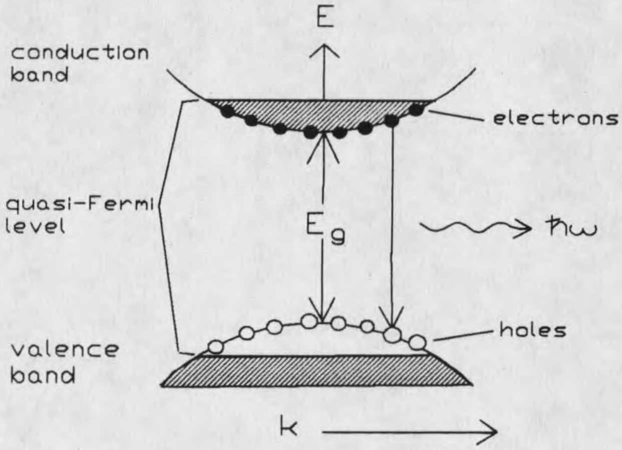

Figure 2. Simplified semiconductor band structure. Stimulated emission causes an electron in the conduction band to recombine with a hole in the valence band.

A standard measure of the performance of a diode laser is the so-called L-I curve, a graph of optical power output vs. injection current (see Figure 3). An important quantity which is derived from this curve is the threshold current. When the laser is operated below threshold, spontaneous emission dominates the optical output and the intensity is relatively low. As lasing commences, the intensity increases dramatically. The threshold current is often found by extrapolating the large-slope portion of the curve back to zero intensity, as indicated in Figure 3.

Another characteristic of laser diodes is that the output wavelength varies with temperature (see Figure 4). Each short segment represents a slight shift in wavelength caused by variation of the index of refraction with temperature and the change in cavity length due to thermal expansion. The latter causes a wavelength shift because the laser wavelengths occur at longitudinal modes of the cavity, and these modes depend on cavity length. There is an overall much greater shift of wavelength with temperature caused by the variation of the bandgap with temperature.

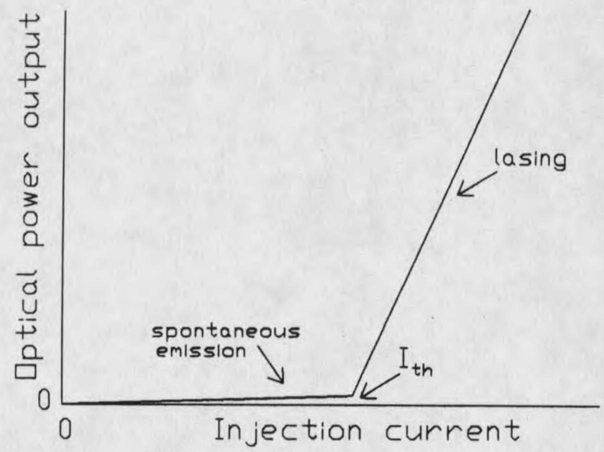

Figure 3. Graph of optical power output vs. injection current (L-I curve).

It should be noticed that the lasing wavelength changes abruptly at certain temperatures. Over a small range of temperature, two modes compete for the available power, and the laser may switch back and forth between these two modes. This is called mode hopping and it is the subject of this study.

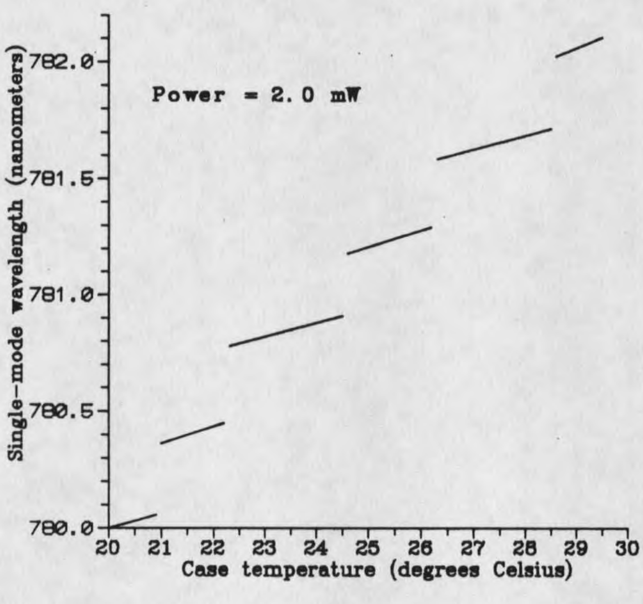

Figure 4. Graph of single-mode wavelength vs. laser case temperature. Mode hopping occurs at the discontinuities.

Motivation for Present Study of Mode Hopping

Mode hopping in semiconductor lasers is undesirable in many applications since it introduces unwanted intensity noise. A prime example is in video disk systems. Mode hopping causes variations in the location of data written to the optical disk because dispersion causes variations in beam direction, possibly necessitating the use of achromatic optics [5]. In addition, the quality of the picture derived from the disk can be degraded by mode hopping since the signal-to-noise ratio is reduced [6]. Video transmission via fiber optics also suffers from intensity noise produced by mode hopping for the same reason [7].

Mode hopping is problematical in other applications as well. In telecommunications, for example, the switching from one mode to another affects the maximum data transmission rate, since different wavelengths have different velocities in single-mode fibers with high dispersion [8]-[10]. Spectroscopy is another area which usually requires wavelength stability better than the 0.2-.3 nm variation that occurs if the laser shifts from one mode to another.

Mode hopping in semiconductor lasers has been studied by many researchers. It has been found that the externally controllable parameters of laser case temperature, injection current, and optical feedback play roles in the occurrence of mode hopping. For example, Gray and Roy [11] monitored dwell times of lasers operating in the bistable regime (complete switching between modes). They showed a qualitative map of single-mode stability as it was affected by current and temperature. Ohtsu and Teramachi [12] found a similar map in studying the power dropout probability. Linke *et al* [7] related the rate of power fluctuations of various depths to the power ratio between the main mode and the largest secondary mode (this ratio is affected by temperature and injection current). Tkach and Chraplyvy [13] found that feedback power ratios of -50 dB or less could induce mode hopping, leading to an increase in intensity noise.

The foregoing examples illustrate how problematic mode hopping is in many applications. There are, therefore, practical motivations for studying mode hopping. In addition, there are many users of diode lasers who would like to be able to know when a laser is mode hopping without resorting to spectrum analyzers or spectrographs. They would also like to be able to eliminate mode hopping without having to modify the laser or to use elaborate external optics or electronics. Finally, of course, the physicist wants to know when and why mode hopping occurs.

Statement of Research Goals

The problem faced at the beginning of this study was therefore two-fold: A non-spectroscopic means of detecting mode hopping was sought, and the conditions under which mode hopping occurs were to be studied with a view to finding a way of controlling it. Chapter II describes, for a laser operating with constant current, a simple method for detecting and quantifying mode hopping by measuring the intensity noise generated while mode hopping is occurring. In

Chapter III, it is shown that there are specific combinations of injection current and case temperature which lead to mode hopping. A stability map reveals the periodicity of these combinations. This observation leads to a method of controlling mode hopping. This periodicity and other features of the stability map are explained in Chapter IV in terms of a two-mode model, taking into account the dynamics of the mode hopping and of the detection system response. Rate equations are developed and solved, and theoretical predictions are made and compared with the experimental results. Chapter V discusses the application of these ideas and techniques to other semiconductor lasers. Finally, Chapter VI concludes the discussion with some comments regarding detection and control of mode hopping.

Chapter II

EXPERIMENTAL SETUP AND PROCEDURE

Description of Setup

Mode hopping in diode lasers was studied using the experimental arrangement shown in Figure 5. A Mitsubishi ML 4402 GaAs index-guided laser was housed in an ILX Lightwave Model 4412 laser mount. The laser mount held the laser against a 2 mm thick aluminum plate. Thermoelectric modules in good thermal contact with the plate allowed heating or cooling of the laser. The temperature of the plate (and hence the case temperature of the laser) was monitored by a calibrated thermistor. The laser mount, glass plate and photodiode were mounted on a 30 cm x 20 cm x 2.5 cm aluminum block to ensure rigidity. This block, resting on a soft foam block for vibration isolation, was placed on an optical table fitted with rigid legs. A foam-lined wooden box with temperature control covered the apparatus to provide secondary temperature buffering.

The laser case temperature and injection current were manipulated using a ILX Lightwave Model 3722 laser diode controller. The controller stabilized injection current and case temperature to <20 nA/√Hz and <5 mK, respectively.

A lens in the laser mount was adjusted to produce a collimated beam. One of the two laser beam reflections from the glass plate was collected by a Hewlett-Packard 5082-4203 PIN photodiode reverse-biased at 22 volts with a series resistance of 1 megohm (see Figure 6). The other beam struck a black felt beam stop. The photodiode's output voltage was measured by a Fluke Model 45 digital voltmeter. This voltmeter, capable of registering dc and ac voltages simultaneously, had a 100 kHz bandwidth and was capable of measuring to the nearest microvolt.

The laser beam which exited the wooden box passed through a neutral density filter (typical optical density was 0.9) into a Bausch and Lomb 1.5 meter spectrograph. The slits widths available were 60, 32 and 10 microns, the latter

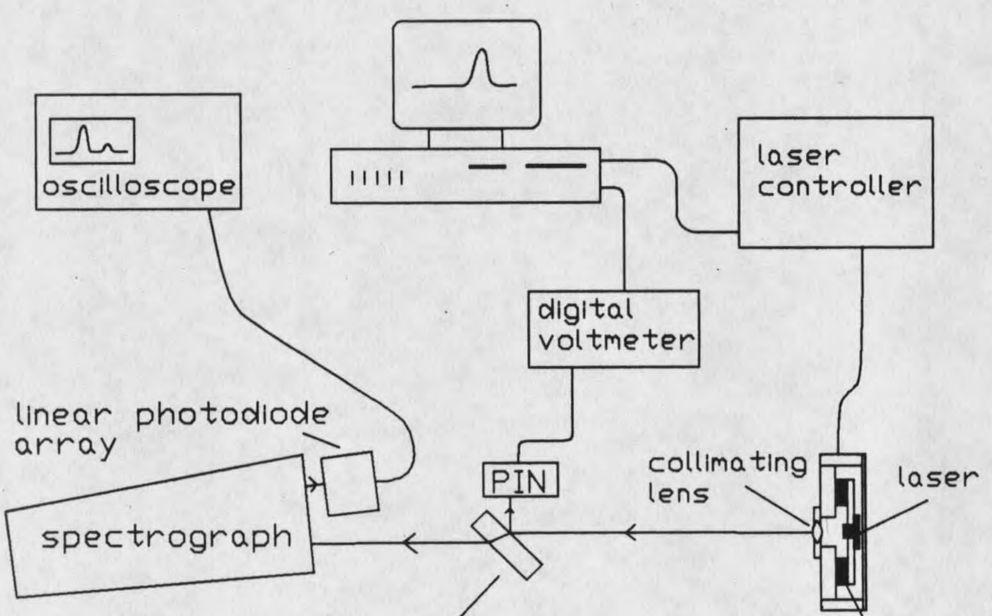

Figure 5. Experimental arrangement for studying mode hopping. The computer was interfaced with both the digital voltmeter and the laser controller.

being used for most observations. The grating, blazed at 490 nm, had 450 lines/mm with a resolving power of around 33,300 in first order. The reciprocal dispersion was 1.48 nm/mm. Details of the calibration of the reciprocal dispersion can be found in Appendix A.

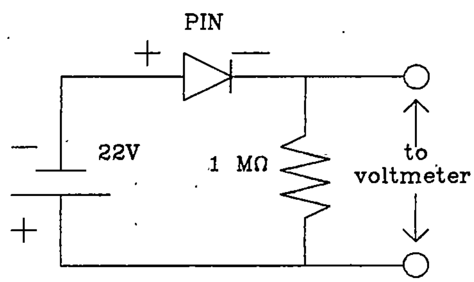

Figure 6. Wiring diagram of PIN photodiode for detection of mode hopping.

A linear photodiode array comprised of 1024 elements spaced 25 microns apart was placed at the output plane of the spectrograph. A digital storage oscilloscope read the array output at 100 Hz to produce a graph of intensity vs. wavelength. The separation between photodiodes in wavelength space was 0.04 nm. This allowed observation of the longitudinal mode spectrum of the laser, since the modes were separated by 0.30 nm. A sample spectrum showing the laser operating with multiple modes is shown in Figure 7.

Optical feedback was minimized by canting all optical surfaces so that back-reflections of the laser beam did not reenter the laser (this included the mirror-like spectrograph slits [3],[14]). This was important, since, as was previously noted, very little feedback was required to cause increased noise.

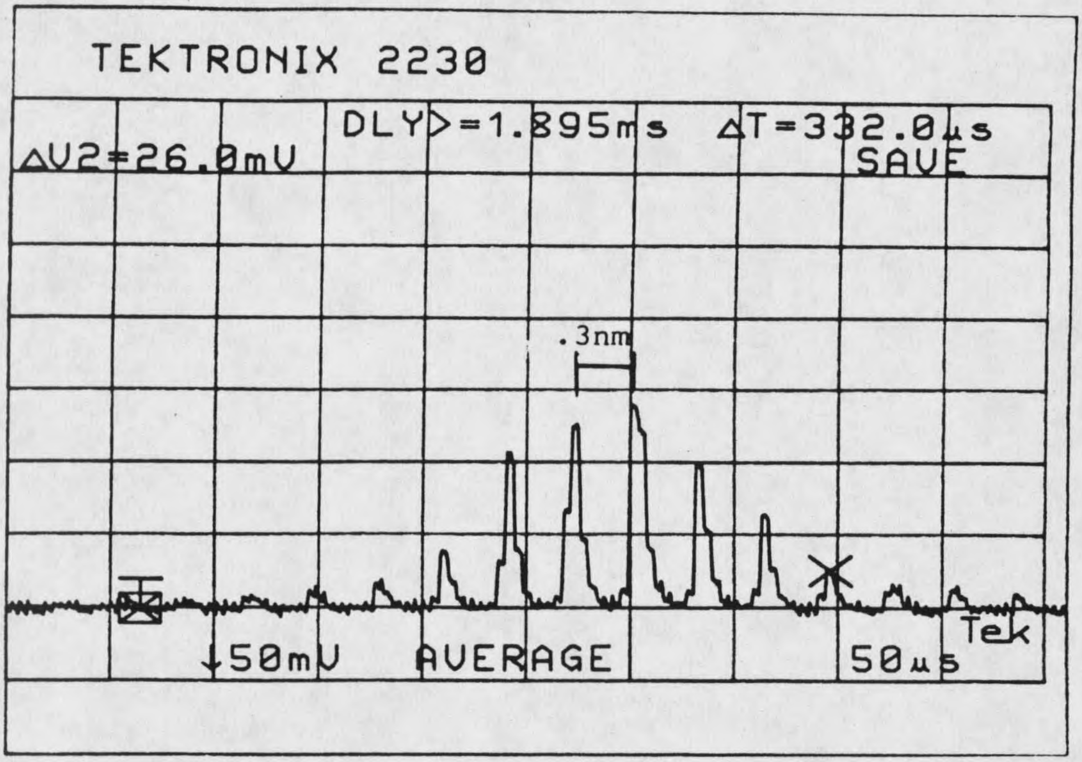

Figure 7. Sample spectrum from linear photodiode array. Short horizontal line segments are individual diodes. Wavelength increases to the left.

<u>Correlation of Mode Hopping with PIN AC Voltage</u>

As the injection current and case temperature were varied, the mode hopping could be observed on the oscilloscope. Simultaneously, the ac voltage produced by the PIN photodiode was noted. There was a strong correlation between the size of the ac signal and the extent of mode hopping: When the laser was mode hopping, the ac signal was significantly elevated compared to its value when the laser was operating in a stable, single mode.

Automated Data Acquisition

Data acquisition was automated by interfacing an AT&T Model 6300 Plus computer with the voltmeter and with the laser controller via a National Instruments GPIB interface card and software. Using programs written in QuickBasic 4.0, the computer incremented the injection current from a given initial value by 0.05 ma steps while holding the case temperature constant. The ac and dc voltmeter readings at each current setting was recorded by the computer in a file whose name was coded to represent the case temperature. A 3-second settling time after the current was changed allowed the voltmeter reading to equilibrate, as changing the injection current changed the intensity which in turn caused a large ac spike which was unrelated to mode hopping. The laser spectrum was observed after the settling period. After the reading corresponding to the highest current was taken, the computer reset the current to the initial value. The controller was commanded to increase the temperature of the laser by 0.1°C. The computer then waited 3 minutes to allow the temperature to stabilize, after which the process was repeated.

CHAPTER III

RESULTS

Peak in AC Voltage vs. Current Graph

When the ac voltage was plotted vs. the injection current for a given constant case temperature, very often a peak was seen, as shown in Figure 8. As was mentioned previously, this peak coincided with the occurrence of mode

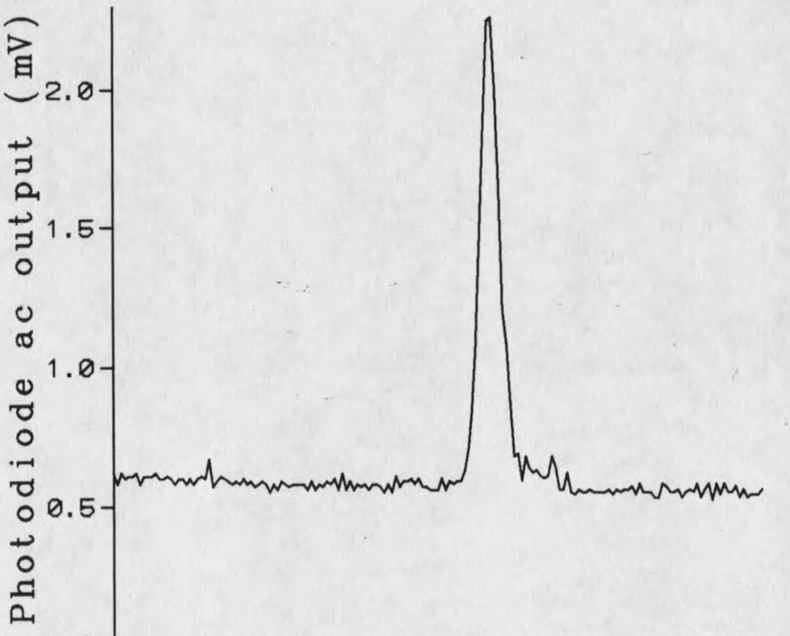

Figure 8. Plot of PIN photodiode ac voltage vs. injection current at constant temperature. The peak occurs when mode hopping is most vigorous.

hopping. The relatively flat parts of the graph correspond to the laser running in a single stable mode. Reasons for the increase in ac voltage during mode hopping will be given in the theoretical discussion in Chapter IV.

The ac signal is unambiguously tied to the occurrence of mode hopping. Therefore, this method is a simple, non-spectroscopic means of detecting the occurrence of mode hopping in semiconductor lasers. As will be discussed in Chapter V, this method has been used on other semiconductor lasers of varying wavelengths with great success: When the injection current and laser case temperature are held constant, the elevation of the ac signal always indicates that mode hopping is occurring.

Grand Stability Map

It was observed that the peak of the ac signal occurred at lower injection currents if the laser case temperature was raised. It was also noted that separate, distinct sets of peaks occurred for different ranges of temperatures. In order to get an overall perspective of the trends being observed, the graphs were plotted in an offset, hidden-line fashion as described in Appendix C. Since the curves were taken in constant increments of temperature, each successive curve was offset from the preceding curve by a constant amount. The vertical axis was labelled to correspond to the temperature at which each curve was taken. The result of this procedure, shown in Figure 9, is called the "grand stability map".

Some features of the map which may be noted are as follows: (1) The ac

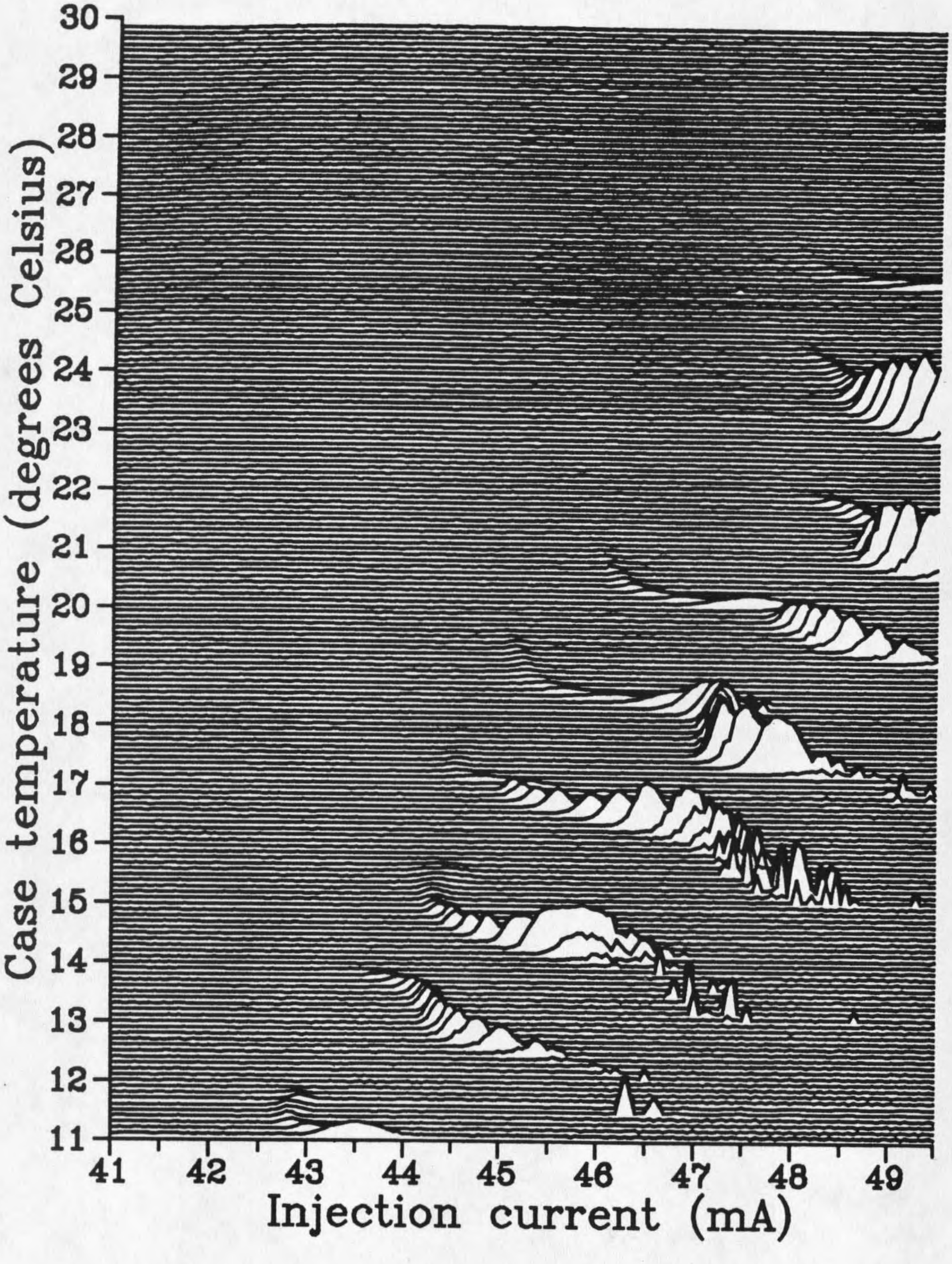

Figure 9. Stability map. Plots of ac voltage vs. current taken at different temperatures are plotted in an offset, hidden-line fashion.

signal peaks form sets of "mountain ranges" which have a negative slope in the temperature-current plane. (2) The centers of the ranges themselves lie on a line of positive slope. (3) The ranges are of finite extent, the upper edges lying roughly along one line, the lower edges lying roughly along another. (4) Each range consists of fairly smooth peaks at one end with a transition to rather more jagged peaks at the other. Finally, (5) there are isolated, jagged peaks which occur along the same line as particular ranges. These features, along with the reason for the existence of the ac voltage peak in the first place, will be discussed in Chapter IV.

CHAPTER IV

THEORY AND EXPLANATION OF MAP FEATURES

The Rate Equations

To understand the features of the stability map seen in Figure 9, we begin by turning to the two-mode theory of Yamada [15]. The rate equations which describe the time variation of the intensity of each longitudinal mode are given as:

$$\begin{aligned} \frac{dS_1}{dt} &= (G_1^{(1)} - G_{th} - G_{1(1)}^{(3)} S_1 - G_{1(2)}^{(3)} S_2)\, S_1, \\ \frac{dS_2}{dt} &= (G_2^{(1)} - G_{th} - G_{2(2)}^{(3)} S_2 - G_{2(1)}^{(3)} S_1)\, S_2, \end{aligned} \qquad (1)$$

where S_m ($m = 1,2$) is the number of photons per unit volume in mode m, and $G_m^{(1)}$, $G_{m(m)}^{(3)}$ and $G_{m(n)}^{(3)}$ ($m \neq n$) are the linear gain, self-saturation and cross-saturation coefficients, respectively. G_{th} is the loss due to absorption, diffraction and coupling of the radiation out of the cavity through the facets. Expressions for these coefficients are given in Appendix A. The photon number is just a convenient way to represent the mode intensity, the relation being

$$S_m = \frac{2\varepsilon_0 n_I^2}{h\nu_m} |E_m(t)|^2 , \qquad (2)$$

where ε_0 is the permittivity of free space, h is Planck's constant, n_I is the index of refraction of the active medium, ν_m is the frequency of the optical field, and $E_m(t)$ is the slowly-varying amplitude of the electric field of mode m. After some algebraic manipulation (see Appendix A), we obtain a dimensionless form of the rate equations which will have a form suitable for solution by methods to be discussed later. The rate equations are:

$$\begin{aligned} \frac{dE_1}{d\tau} &= (a_1 - E_1^2 - \xi E_2^2)E_1, \\ \frac{dE_2}{d\tau} &= (a_2 - E_2^2 - \xi E_1^2)E_2, \end{aligned} \tag{3}$$

where

$$\begin{aligned} a_1 &= \frac{(G_1^{(1)} - G_{th})h\nu}{2\varepsilon_0 n_I^2 G_{1(1)}^{(3)}}, \\ a_2 &= \frac{(G_2^{(1)} - G_{th})h\nu}{2\varepsilon_0 n_I^2 G_{1(1)}^{(3)}}, \\ \xi &= \frac{G_{1(2)}^{(3)}}{G_{1(1)}^{(3)}}, \\ \tau &= \frac{h\nu}{\varepsilon_0 n_I^2 G_{1(1)}^{(3)}} t. \end{aligned} \tag{4}$$

The quantities a_1 and a_2 are called pump parameters, ξ is the mode coupling coefficient, and τ is the dimensionless time.

We note that quantum fluctuations should play a role in the behavior of the laser [11],[16],[17]. Spontaneous emission happens randomly and is the major source of fluctuations which plays a role here. We incorporate these fluctuations by adding Langevin noise terms $q_i(\tau)$ to the rate equations:

$$\frac{dE_1}{d\tau} = (a_1 - E_1^2 - \xi E_2^2)E_1 + q_1(t),$$
$$\frac{dE_2}{d\tau} = (a_2 - E_2^2 - \xi E_1^2)E_2 + q_2(t), \tag{5}$$

where the $q_i(\tau)$ obey the following conditions:

$$\langle q_i^*(\tau)\, q_j(\tau')\rangle = 2\delta_{ij}\delta(\tau-\tau'),$$
$$\langle q_i(\tau)\rangle = 0. \tag{6}$$

The first condition says that the two modes fluctuate independently: They are uncorrelated. It also says that, for a given mode, events at one time are uncorrelated to preceding events (this condition is called the Markoffian approximation [18]). The second condition simply says that the fluctuations in a mode average to zero. In addition, we assume that the q_i obey Gaussian statistics.

The Potential

Equations 5 above are called Langevin equations. The E_i are stochastic variables whose fluctuations are distributed according to a distribution function $p(E_1,E_2,t)$ [16]. This distribution is a joint probability density such that $p(E_1E_2,t)dE_1dE_2$ is the probability of finding the laser at time t having the electric fields within E_1+dE_1 and E_2+dE_2. With the preceding assumptions about the correlations of the q_i, the Langevin equations can be solved (for the average quantities) by solving the related diffusion equation for $p(E_1,E_2,t)$ called the Fokker-Planck equation. Following the procedure given by M.-Tehrani and Mandel [16], we write the (normalized) electric fields as sums of real and imaginary parts, i.e., $E_1 = x_1 + ix_2$ and $E_2 = x_3 + ix_4$. We then have $p(x_1,x_2,x_3,x_4)$ which satisfies the Fokker-Planck equation:

$$\frac{\partial p}{\partial \tau} = \sum_{i=1}^{4}\left(p\frac{\partial A_i}{\partial x_i} - \frac{\partial^2 p}{\partial x_i^2}\right) \tag{7}$$

where

$$\begin{aligned} A_1 &= [a_1-(x_1^2+x_2^2)-\xi(x_3^2+x_4^2)]x_1, \\ A_2 &= [a_1-(x_1^2+x_2^2)-\xi(x_3^2+x_4^2)]x_2, \\ A_3 &= [a_2-(x_3^2+x_4^2)-\xi(x_1^2+x_2^2)]x_3, \\ A_4 &= [a_2-(x_3^2+x_4^2)-\xi(x_1^2+x_2^2)]x_4. \end{aligned} \tag{8}$$

The time-independent solution to this differential equation, obtained by setting $\partial p/\partial\tau = 0$, is given by

$$p = \frac{1}{Q}\exp[-U(x_1,x_2,x_3,x_4)] \ , \tag{9}$$

where

$$\begin{aligned} U = {} & \frac{1}{4}[(x_1^2+x_2^2)^2+(x_3^2+x_4^2)^2]-\frac{1}{2}a_1(x_1^2+x_2^2) \\ & -\frac{1}{2}a_2(x_3^2+x_4^2)+\frac{1}{2}\xi(x_1^2+x_2^2)(x_3^2+x_4^2) \end{aligned} \tag{10}$$

is a potential and Q is the normalizing factor such that $\int_0^\infty p(I_1,I_2)dI_1dI_2 = 1$. If we make the identifications $x_1^2+x_2^2 = I_1^2$ and $x_3^2+x_4^2 = I_2^2$, where I_1 and I_2 are dimensionless intensities, we can write the potential as

$$U = \frac{1}{4}I_1^2+\frac{1}{4}I_2^2-\frac{1}{2}(a_1I_1+a_2I_2)+\frac{1}{2}\xi I_1I_2 \ . \tag{11}$$

The shape of this potential varies with a_1 and a_2. When $a_1/a_2>\xi$, the potential has a single minimum at $(I_1,I_2) = (a_1,0)$ (considering only non-negative values of I_1

and I_2). This corresponds to the single stable solution of Eqn. 7. The laser oscillates stably about this solution, with spontaneous emission fluctuations giving rise to variations in the intensity. This is called mode partitioning. If, on the other hand, $1/\xi<a_1/a_2<\xi$, then there are two minima, corresponding to two stable solutions, one at $(a_1,0)$ and another at $(0,a_2)$, with a saddle point between them. The laser oscillates about either of these solutions, with spontaneous emission fluctuations occasionally driving the laser from one state to the other. This is called mode hopping.

It should be noted for future reference that the height of the saddle point relative to the depths of the minima increases with the pump parameters, the height of the saddle point relative to the minimum being given by [19]

$$\Delta U_i = \frac{1}{4}a_i^2-\frac{(a_1^2-2\xi a_1 a_2+a_2^2)}{4(1-\xi^2)}\ , i=1,2. \qquad (12)$$

This will have implications for the rate of switching between modes.

Total Intensity Noise

We wish to find the rms fluctuations of the total intensity (total intensity noise) as a function of injection current in order to compare to the measured results, as we expect that the peak in ac voltage is due to a peak in the total intensity noise. Writing the total intensity $I = I_1+I_2$, we find that

$$\begin{aligned}\langle(\Delta I)^2\rangle &\equiv \langle I^2\rangle-\langle I\rangle^2 \\ &= \langle I_1\rangle^2-\langle I_1^2\rangle+2\,[\langle I_1\rangle\langle I_2\rangle-\langle I_1 I_2\rangle]+\langle I_2\rangle^2-\langle I_2^2\rangle,\end{aligned} \qquad (13)$$

where ⟨⟩ denotes average. Using the joint probability density $p(I_1,I_2)$, we can determine the various moments of the intensities above. We have

$$\langle I_m^r I_n^s \rangle = \frac{1}{Q}\int_0^\infty dI_1\, dI_2\, I_m^r I_n^s \exp[-U(a_1, I_1, a_2, I_2, \xi)] \quad . \tag{14}$$

Details of the integration may be found in Appendix A. Numerical integration is required.

Nonlinear Gain Model

In order to calculate the total intensity noise, we must have numerical values for the pump parameters and the coupling coefficient. Going to Eqns. 20 in Appendix A for the coefficients appearing in the rate equations (Eqns. 4), we note that the form of $G_m^{(1)}$-G_{th} is that of an inverted parabola whose vertex shifts upward with carrier density. As is noted in Appendix A, the carrier density does vary a little with injection current. Thus, the net gain increases with injection current.

The wavelengths of the longitudinal modes and the peak of the gain profile also shift with injection current (see Appendix F). This is due to the rise in temperature of the active region, or junction, as a result of joule heating. This causes thermal expansion of the laser cavity, thereby shifting the mode wavelength [20]. In addition, the bandgap energy, which is responsible for the peak wavelength of the gain profile, is also a function of temperature [21]-[22]. We can express the wavelengths as

$$\begin{aligned}\lambda_1 &= \lambda_1^0+v_\lambda(J-J_0)\,,\\ \lambda_2 &= \lambda_2^0+v_\lambda(J-J_0)\,,\\ \lambda_p &= \lambda_p^0+v_p(J-J_0)\,,\end{aligned} \tag{15}$$

where λ_1 is the wavelength of mode 1, λ_2 is the wavelength of mode 2, λ_p is the wavelength of the gain peak, J is the injection current, J_0 is the current for which the gain peak wavelength is centered between the mode wavelengths, and λ_2^0, λ_1^0 and λ_p^0 are the various wavelengths when $J = J_0$. v_p and v_λ are the rate of change with current of the peak gain and mode wavelengths, respectively. The wavelengths obey the condition $\lambda_p^0-\lambda_1^0 = \lambda_2^0-\lambda_p^0$.

By including the dependence of the carrier density and the wavelengths on injection current, we can write the pump parameters in a form which takes into account both the parabolic form of the gain and the relative changes of the gain peak and mode wavelengths with injection current, as well as the increase in net gain with current. We write the following expression for the gain profile as a function of wavelength:

$$a = a'(J-J_{th})-c(\lambda-\lambda_p)^2\,, \tag{16}$$

where a′ is the height of the gain peak, J_{th} is the threshold current, c is related to the curvature of the parabola, λ_p is the wavelength of the gain peak and λ is an arbitrary wavelength. Then a_1 and a_2 are the values of the gain of modes 1 and 2, respectively, at the corresponding wavelengths λ_1 and λ_2. Written in a convenient form, the pump parameters are:

$$
\begin{aligned}
a_1 &= a_0 \frac{(J/J_{th}-1) - k\left[\dfrac{\Delta\lambda}{2} + \Delta v\,(J-J_0)\right]^2}{(J_0/J_{th}-1) - k\left(\dfrac{\Delta\lambda}{2}\right)^2}, \\
a_2 &= a_0 \frac{(J/J_{th}-1) - k\left[\dfrac{\Delta\lambda}{2} - \Delta v\,(J-J_0)\right]^2}{(J_0/J_{th}-1) - k\left(\dfrac{\Delta\lambda}{2}\right)^2},
\end{aligned}
\tag{17}
$$

where $a_0 = a_1(J = J_0) = a_2(J = J_0)$, $\Delta v = v_p - v_\lambda$, and $\Delta\lambda = \lambda_2^0 - \lambda_1^0$. The value of k is chosen to give a width of the gain profile above threshold of 5 nm based on the width of the spectrum in Figure 7.

The relationships between the gain values and the injection current are illustrated in Figure 10. The gain profile shifts upward and toward longer

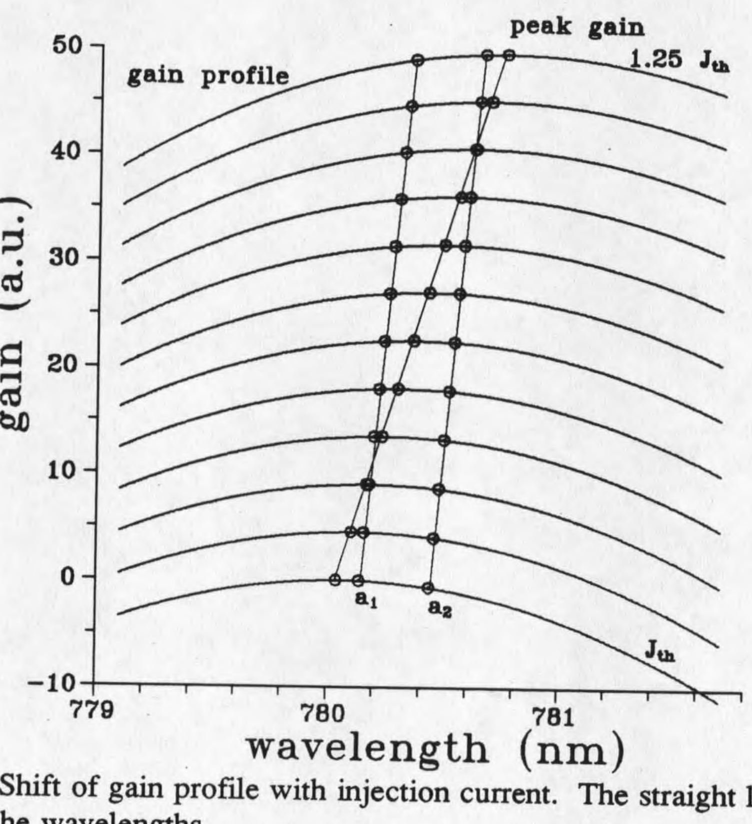

Figure 10. Shift of gain profile with injection current. The straight lines show the shift of the wavelengths.

wavelengths as the injection current increases. Since the gain peak shifts more rapidly than the modes, the gain of mode 1 is first larger than that of mode 2 ($a_1>a_2$), then the two gains are equal ($a_1=a_2$), and finally mode 2 becomes dominant ($a_2>a_1$).

The last quantity needed to carry out the calculations of the average intensities and the total noise is the mode coupling coefficient ξ. From Eqn.4, and from the expressions given in Appendix A, we find that

$$\xi = \frac{4}{3}/[1+(2\pi c\tau_{in}\Delta\lambda/\lambda^2)^2] \ , \tag{18}$$

where c is the speed of light in vacuum, τ_{in} is the intraband relaxation time (about 0.1 ps), $\Delta\lambda$ is the wavelength difference between modes 1 and 2 (0.3 nm), and λ is the laser wavelength (780 nm). In this case, $\xi = 1.3$, which corresponds to strong coupling as discussed by Sargent, Scully and Lamb [22].

Explanation of Features

Peak in AC Voltage

With the foregoing theory in place, we are in a position to explain many of the features of the stability map. The first feature we consider is the peak in the PIN photodiode ac voltage which occurs when mode hopping is taking place. Armed with the analytical expressions for a_1 and a_2 in terms of the injection current, we calculate the average intensities and the total noise as functions of current. The results are shown in Figure 11, where it was assumed that $J_0 = 1.3\ J_{th} = 63.5$ ma.

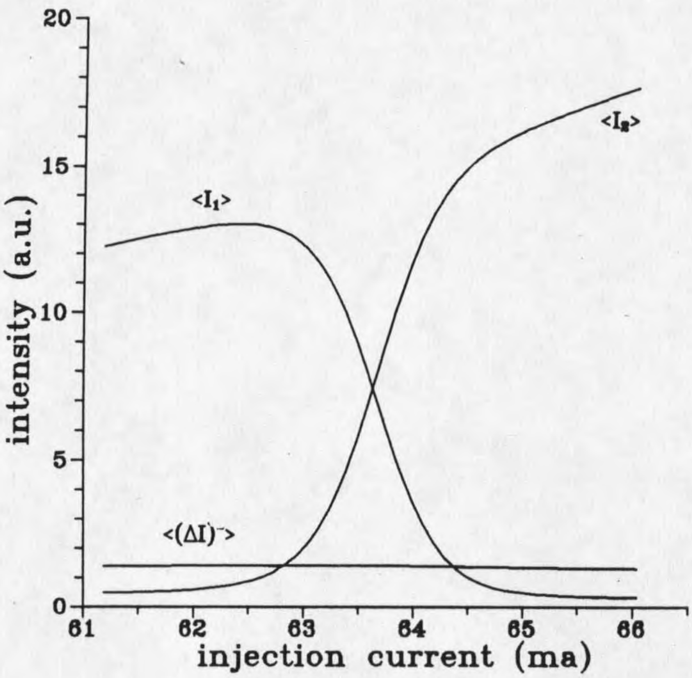

Figure 11. Theoretical average intensities vs injection current.

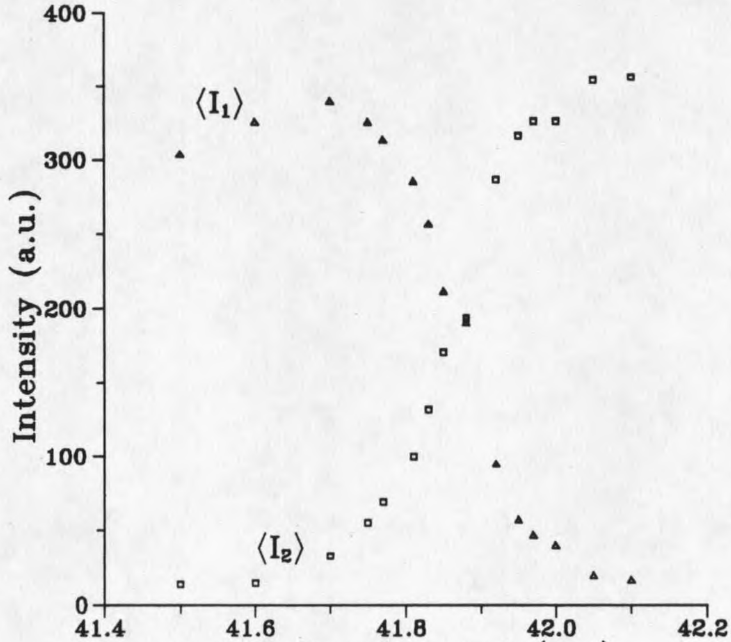

Figure 12. Plot of experimental average intensities vs. injection current.

The intensities can be seen to exchange places in the vicinity of J_0. These results were tested experimentally by averaging the spectrum (as seen on the digital storage oscilloscope placed in average mode) over long periods while the injection current was held constant. Spectra were taken for various values of current. The intensities are plotted in Figure 12. As can be seen by comparing these results with those of Figure 11, there is good agreement of form between theory and experiment.

The total noise is also plotted vs. current in Figure 11. It is constant at the resolution of the plotter. This result is surprising, since we expected the total noise to exhibit a dramatic peak during mode hopping. Clearly, we must look elsewhere for the source of the strong ac signal seen in Figure 8.

A possible resolution of this paradox begins with noting the experimental results of Ohtsu and Teramachi [12], who found that the low-frequency spectral distribution of the noise is Lorentzian with a half-power width (cutoff frequency) which varies strongly with the ratio of the average intensities. This was presented in the form of a graph of cutoff frequency vs. $\langle I_1 \rangle / \langle I_2 \rangle$, with the ratio increasing from unity. This variation of the spectral width may play a role in the ac voltage because of the detection system's finite bandwidth. This will be discussed later.

Meg Hall of our laboratory has observed experimentally this variation of the noise spectral width with intensity ratio , at least in a qualitative way. Shown in Figure 13 are one-shot time series of the photodiode voltage (proportional to the total intensity) taken at two different injection currents. The lower figure (curve A) was taken when the ac voltage was slightly elevated above the background level, and the ratio of average intensities was relatively large. The upper figure (curve B) was taken near the peak ac voltage, when the average intensities were approximately equal. Distinct differences in the time scale and magnitude of the fluctuations are evident: In the upper figure, the total intensity is seen to alternate between two distinct levels, spending substantial amounts of time at each level before switching to the other level. This behavior has been seen by others [8],[11],[16],[19]. In contrast, the lower figure shows very frequent and often partial switching between intensities.

When Hall applies the fast Fourier transform technique [23] to the time

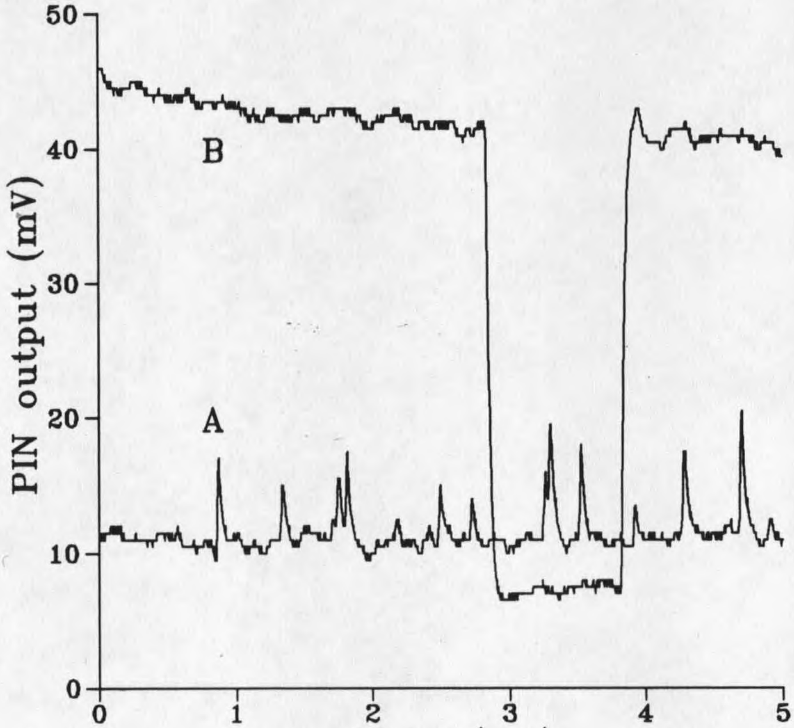

Figure 13. Oscilloscope traces showing total intensity fluctuations. Curve B was taken at the peak of the ac signal, curve A at a low value.

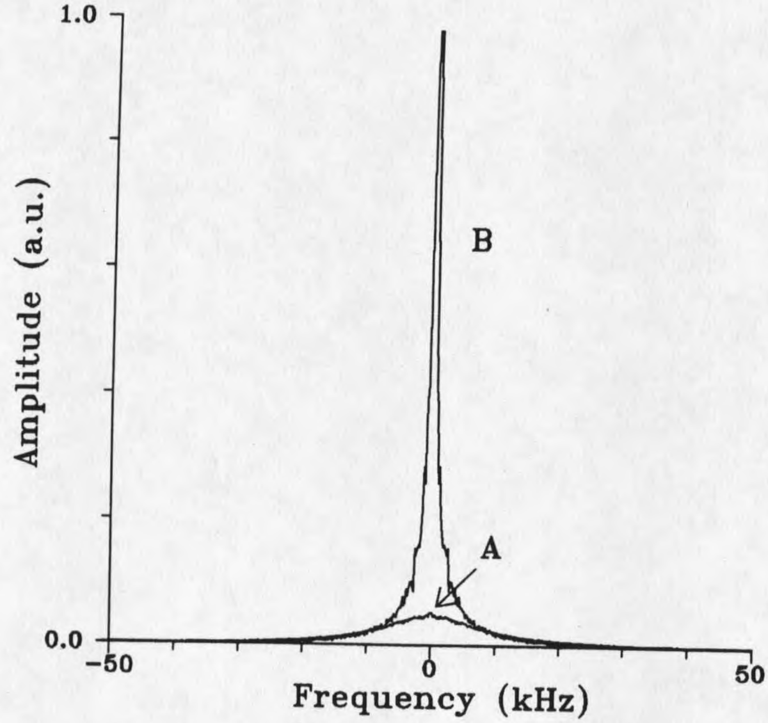

Figure 14. Fast Fourier transforms of the time series shown in Figure 13. Note large difference in width and height of spectral densities.

series, a dramatic difference in the spectral distribution of the noise is found. Shown in Figure 14 are the Fourier transforms of the corresponding time series. When the ratio of the intensities of the two modes was large (curve A), the cutoff frequency, or half-width, was also large, corresponding to the wide range of the magnitude and frequency of the intensity fluctuations. When the intensities were of similar magnitude (curve B), the spectral distribution became much narrower . This is understandable, since the intensity varies mostly between two levels and there is not an extremely large variation in the times spent in either level.

We return to the question of the ac voltage peak. The constancy of the total intensity noise, coupled with the variation in spectral width just discussed, suggests that the portion of the Lorentzian noise spectrum which falls within a given frequency bandwidth changes. Because the detection system has a finite bandwidth, it can respond to only part of the complete total intensity noise spectrum. This is illustrated schematically in Figure 15.

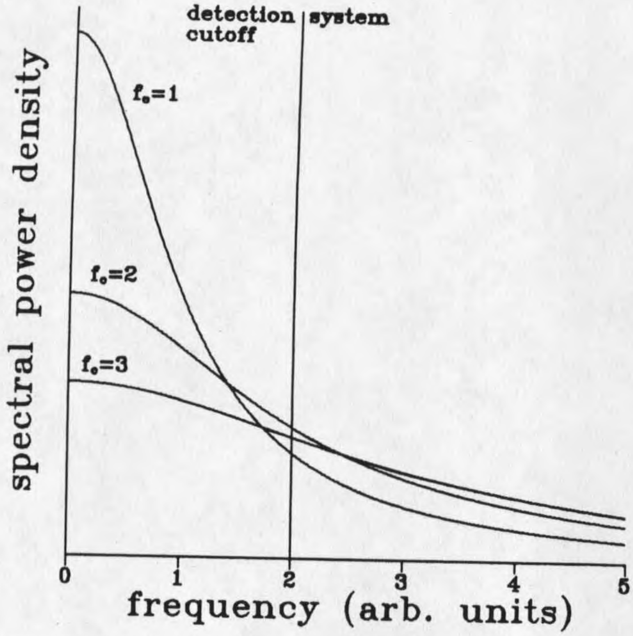

Figure 15. Schematic illustration of variation of spectral density within detection system window.

As the spectral width narrows, the peak of the spectrum increases to keep the total noise (the area under curve) constant. Thus, the amount of noise seen by the detection system increases. The ac voltage should be largest when the spectrum is narrowest, which occurs when the intensities are equal. This is indeed what is observed.

Calculation of the ac voltage based on these ideas leads to the graph shown in Figure 16. Comparison of this curve to that of Figure 8 reveals excellent agreement of form. Details of the calculations may be found in Appendix G.

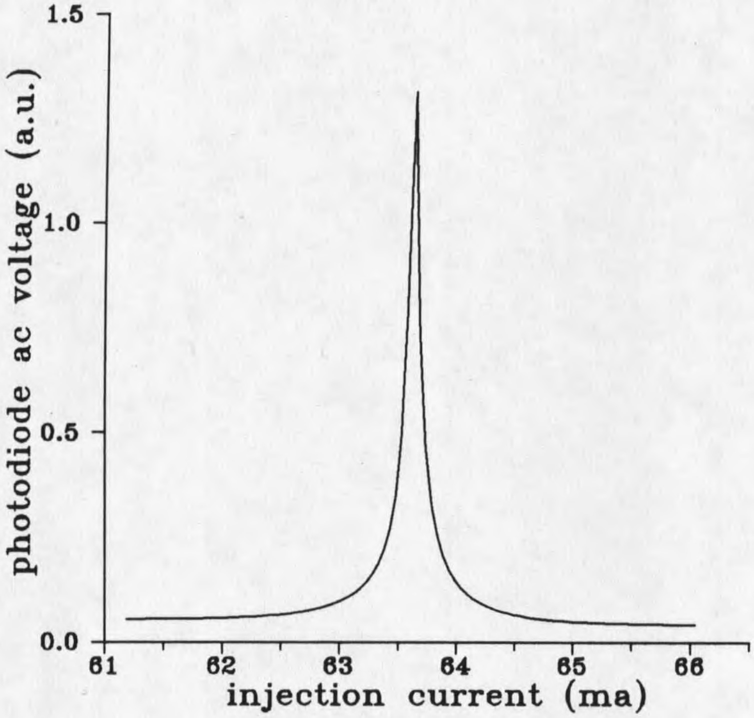

Figure 16. Plot of theoretical ac voltage vs. injection current based on shifting Lorentzian model.

Mountain Ranges

Another feature of the stability map is that the injection current at which the peak of mode-hopping activity occurred shifts to smaller values with increasing temperature, giving rise to the "mountain range" appearance. To understand this, we recall that mode hopping occurs when the peak of the gain profile lies nearly centered between two modes. This occurs because of the dependence of wavelengths on injection current. However, as is shown in Appendices D-E, specific injection currents correspond to specific junction temperatures, and it is actually the junction temperature which determines the relative values of the wavelengths (see Appendix F). We therefore expect that the mountain ranges should lie along lines of constant junction temperature. However, the junction temperature depends not only on the case temperature but also on injection current, due primarily to joule heating [20], [24]. To achieve the same junction temperature at higher case temperature, the current must be reduced. Thus, when the case temperature increases, the peak of mode hopping occurs at a reduced injection current. This is why the mountain ranges have a negative slope. Figure 17 shows an experimentally measured line of constant junction temperature superimposed on the stability map (dashed line). The line qualitatively parallels the slope of the mountain ranges in confirmation of the hypothesis. See Appendix D for details.

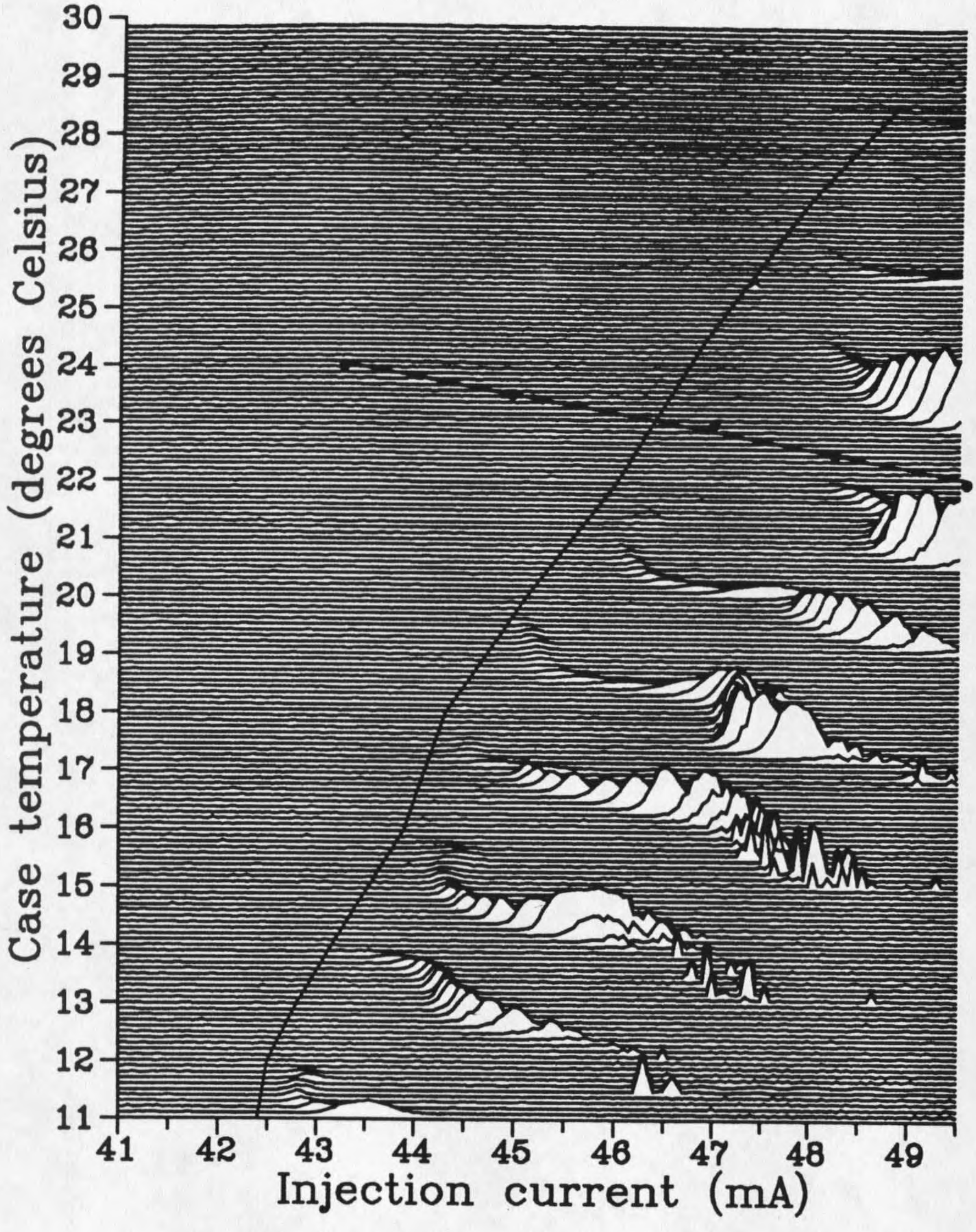

Figure 17. Stability map. Solid line marks boundary between multimode and single mode operation. Dots are data and dashed line is best-fit line of constant junction temperature.

Periodicity of Ranges

Still another feature we notice in Figure 9 is that the mountain ranges occur repeatedly, the location shifting (positively) with temperature. As was mentioned earlier, the mode and gain peak wavelengths depend on the junction temperature. The gain peak periodically overtakes the modes as the junction temperature increases (see Appendix F). This is schematically illustrated in Figure 18. The wavelength of the gain peak shifts with temperature more quickly than the longitudinal mode wavelengths do. This effect can also be seen in Figure 4. The individual mode wavelengths (short line segments) shift at a rate of 0.065 nm/°C (in agreement with Chambliss and Johnson [25]) while the overall wavelength shift rate of the gain profile is 0.208 nm/°C (which compares well with Wieman [3] and Lee et al [26]). The former rate is caused primarily by the change in the index of refraction and by thermal expansion [20], while the latter rate is chiefly due to the decrease in the bandgap with temperature [27].

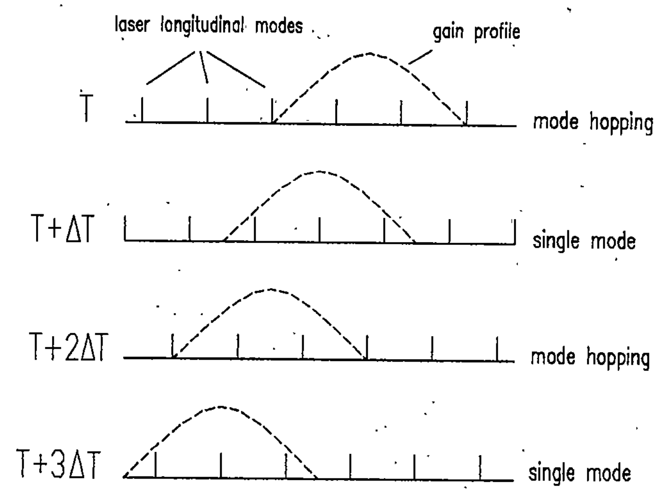

Figure 18. Illustration of shift of gain profile and modes with temperature. The gain profile moves more rapidly. Wavelength increases to the left.

On this basis, we can calculate what the expected separation (in terms of case temperature) between the ranges should be. It is

$$\Delta T = \Delta\lambda/(R_g - R_\lambda), \tag{18}$$

where ΔT is the temperature shift, $\Delta\lambda$ is the longitudinal mode separation, R_g is the rate at which the gain peak shifts with respect to temperature, and R_λ is the longitudinal mode shift rate. For the values given above, we obtain $\Delta T = 2.1°C$. This value is in good agreement with an experimental estimate of $2.1 \pm 0.3°C$ obtained by drawing a line along each of the mountain ranges and noting the vertical separation between the lines.

Finiteness of Ranges, Jagged and Anomalous Peaks

The mountain ranges do not persist indefinitely, but have fairly definite ends, although there are peaks which do occur isolated from the mountain ranges. It may be noted that the low-current ends of the mountain ranges seem to follow a smooth line. This line coincides closely with the transition from multimode to single-mode operation (single-mode defined as the main mode being 20 times larger than the largest side mode [26]). This transition line is shown superimposed on the stability map (Figure 17) as a solid line. To the left of this line, the laser has two or more modes oscillating simultaneously. Changing the junction temperature causes the distribution of modes to shift (mode "oozing"), but there is no abrupt switching. However, to the right of the transition line, single mode operation occurs except during mode hopping. Thus, we find that mode hopping occurs only when the laser is operating in the single-mode regime.

The high-current end of the mountain ranges occurs because the probability of switching becomes quite low even when the gain profile is centered between the modes. This is due to the aforementioned fact that the height of the saddle point of the potential relative to the depth of the minimum increases with pump parameter (and therefore with injection current). As the "barrier" between the two states increases, switches become much less likely. They do occur, but the rapid back-and-forth switching does not take place. This is consistent with the prediction of Wang et al [28], who showed that the time should increase exponentially with the barrier height. This trend of increase of dwell time with pump parameter has been experimentally demonstrated by Gray and Roy [11]. This means that the ac voltage will exhibit infrequent spikes in this regime, but will otherwise display quiescent behavior.

The elevation of the barrier height with injection current also accounts for the transition in a mountain range from smooth peaks to jagged ones. The jagged peaks occur because the switching has become episodic rather than frequent. This produces a large irregularity in the ac signal.

CHAPTER V

ADDITIONAL RESULTS

Heather Thomas of our laboratory obtained stability maps for a variety of semiconductor lasers; some of the results are shown in Figure 19. Going clockwise from the upper left, the lasers are a 1.3 micron Mitsubishi, a 780 nm Mitsubishi, a 780 nm Sharp, and another 780 nm Sharp. The second 780 nm Mitsubishi was the same model number as was used to produce the stability map of Figure 9.

Clearly, stability maps vary considerably from laser to laser, even for lasers of identical model numbers. While some maps demonstrate some of the effects discussed in the previous chapters, it is clear that our simple model is inadequate to explain the rich diversity of patterns seen in Figure 19. However, the stability map remains useful as a means of choosing stable operating parameters. Furthermore, the simple method of mode-hopping detection described previously is useful regardless of the availability of a stability map.

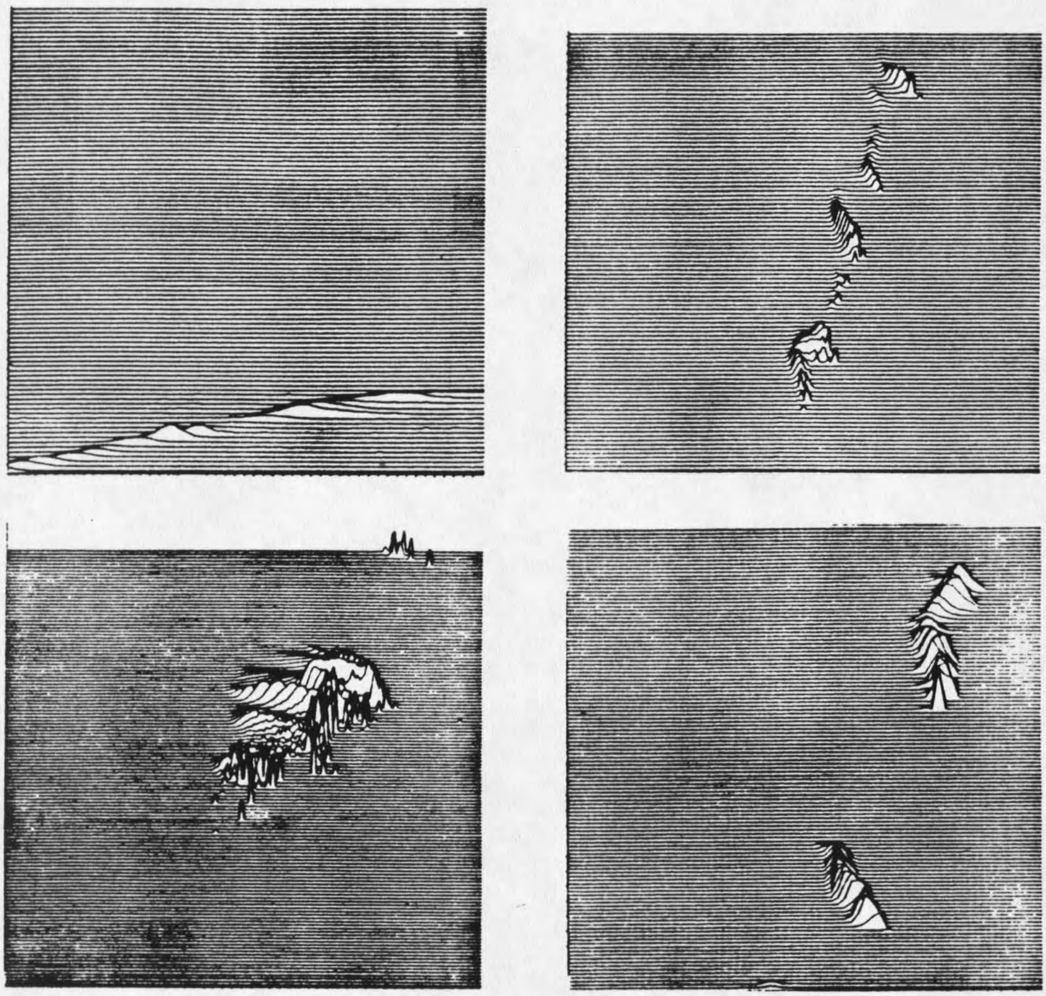

Figure 19. Stability maps of various lasers. See text for details.

CHAPTER VI

CONCLUSION

Semiconductor lasers have found a wide range of applications due to the variety of wavelengths available, the compact size, low price and the ease of control. The rapid switching known as mode hopping gives rise to undesirable intensity noise which can limit the performance of these lasers in some applications. The level of intensity noise has been shown to be directly correlated to the occurrence of mode hopping. We have demonstrated a simple, non-spectroscopic method of detecting the occurrence of mode hopping by using the increase in intensity noise as an indicator. We have also shown that mode hopping occurs for specific values of laser case temperature and injection current. This means that mode hopping can be eliminated by careful control of these parameters. The stability map (distinct for each laser) is a reliable means of determining which values of the parameters will result in stability. These findings should be found useful to anyone for whom mode hopping is a potential problem.

This work was supported by grants from ILX Lightwave, Inc.

APPENDICES

APPENDIX A

DETAILS OF MODEL DEVELOPMENT AND CALCULATION OF INTENSITY NOISE

Closely following the development by Yamada [15], the rate equations are

$$\begin{aligned}\frac{dS_1}{dt} &= (G_1^{(1)} - G_{th} - G_{1(1)}^{(3)} S_1 - G_{1(2)}^{(3)} S_2)\, S_1, \\ \frac{dS_2}{dt} &= (G_2^{(1)} - G_{th} - G_{2(2)}^{(3)} S_2 - G_{2(1)}^{(3)} S_1)\, S_2,\end{aligned} \tag{19}$$

with m,n = 1,2. The coefficients are defined as follows:

$$\begin{aligned} G_m^{(1)} &= \frac{g^{(1)}\xi^{(1)}}{n_I\sqrt{\mu_0\varepsilon_0}}\,[n^{(0)} - n_G^{(1)} - h'(\lambda_m - \lambda_p)^2], \\ G_{m(n)}^{(3)} &= \frac{h\nu_m g^{(1)}\xi^{(3)} 16\pi^2(\tau_{in}/h)^2\langle M\rangle^2}{2\varepsilon_0\sqrt{\varepsilon_0\mu_0}\, n_I^3(1+\delta_{m,n})}\,\frac{n^{(0)} - n_G^{(3)}}{1+(\tau_{in}\omega_n/\lambda_n)^2(\lambda_m-\lambda_n)^2}, \\ G_{th} &= \frac{\xi^{(1)} g^{(1)} (n_{th}^{(0)} - n_G^{(1)})}{n_I\sqrt{\mu_0\varepsilon_0}}. \end{aligned} \tag{20}$$

The various quantities which appear in these expressions are defined as follows:

n_I: Index of refraction.

$\xi^{(1)}, \xi^{(3)}$: Power confinement ratios (not to be confused with the mode coupling factor ξ).

$g^{(1)}$: Slope of linear gain with carrier density.

$n^{(0)}$: Carrier density injected into the active region.

$n_{th}^{(0)}$: Carrier density at lasing threshold.

$n_G^{(0)}$: Carrier density to get positive linear gain.

$n_G^{(3)}$: Carrier density to get positive values of saturation coefficients.

h': Curvature of linear gain profile.

τ_{in}: Intraband relaxation time.

λ_p: Wavelength of peak gain.

λ_m: Wavelength of mode m.

$\langle M \rangle^2$: Square of the dipole moment formed by electron-hole pairs.

The intensity is related to the photon number by

$$S_m = \frac{2\varepsilon_0 n_I^2}{h\nu_m} |E_m(t)|^2 \text{ , m=1,2.} \tag{21}$$

Substitution of these relations into Eqns. 19 yields, after cancellation of common factors,

$$\begin{aligned} \frac{d|E_1|^2}{dt} &= \left(G_1^{(1)} - G_{th} - \frac{2\varepsilon_0 n_I^2}{h\nu_1} G_{1(1)}^{(3)} |E_1|^2 - \frac{2\varepsilon_0 n_I^2}{h\nu_2} G_{1(2)}^{(3)} |E_2|^2\right) |E_1|^2, \\ \frac{d|E_2|^2}{dt} &= \left(G_2^{(1)} - G_{th} - \frac{2\varepsilon_0 n_I^2}{h\nu_2} G_{2(2)}^{(3)} |E_2|^2 - \frac{2\varepsilon_0 n_I^2}{h\nu_1} G_{2(1)}^{(3)} |E_1|^2\right) |E_2|^2. \end{aligned} \tag{22}$$

Assuming that E_1 and E_2 are complex, so that $|E|^2 = E^*E$, we see that

$$\begin{aligned} \frac{d|E|^2}{dt} &= \frac{d(E^*E)}{dt} \\ &= E\frac{dE^*}{dt} + E^*\frac{dE}{dt}, \end{aligned} \tag{23}$$

where * denotes complex conjugates. As may be easily verified for complex numbers A and B, if $A + A^* = B + B^*$, then $A = B$. Here, E^*dE/dt plays the role of A, and 1/2 the right-hand side of Eqn. 22 is B. Thus,we can write

$$\begin{aligned} \frac{dE_1}{dt} &= \frac{1}{2}\left(G_1^{(1)} - G_{th} - \frac{2\varepsilon_0 n_I^2}{h\nu_1} G_{1(1)}^{(3)} |E_1|^2 - \frac{2\varepsilon_0 n_I^2}{h\nu_2} G_{1(2)}^{(3)} |E_2|^2\right) E_1, \\ \frac{dE_2}{dt} &= \frac{1}{2}\left(G_2^{(1)} - G_{th} - \frac{2\varepsilon_0 n_I^2}{h\nu_2} G_{2(2)}^{(3)} |E_2|^2 - \frac{2\varepsilon_0 n_I^2}{h\nu_2} G_{2(1)}^{(3)} |E_1|^2\right) E_2. \end{aligned} \tag{24}$$

If we divide by $(2\varepsilon_0 n_I^2/h\nu)G_{1(1)}^{(3)}$ in both equations, we obtain a normalized form for the rate equations, namely,

$$\begin{aligned} \frac{dE_1}{d\tau} &= (a_1 - E_1^2 - \xi E_2^2)E_1, \\ \frac{dE_2}{d\tau} &= (a_2 - E_2^2 - \xi E_1^2)E_2, \end{aligned} \tag{25}$$

The quantities a_i, ξ and τ are defined by:

$$\begin{aligned} a_1 &= \frac{(G_1^{(1)} - G_{th})h\nu}{2\varepsilon_0 n_I^2 G_{1(1)}^{(3)}}, \\ a_2 &= \frac{(G_2^{(1)} - G_{th})h\nu}{2\varepsilon_0 n_I^2 G_{1(1)}^{(3)}}, \\ \xi &= \frac{G_{1(2)}^{(3)}}{G_{1(1)}^{(3)}}, \\ \tau &= \frac{\varepsilon_0 n_I^2 G_{1(1)}^{(3)}}{h\nu}t. \end{aligned} \tag{26}$$

In obtaining Eqns. 25, we have assumed that $\nu_1 = \nu_2 = \nu$ (a good approximation for the closely-spaced modes of the semiconductor laser). We have also assumed that $G_{1(2)}^{(3)} = G_{2(1)}^{(3)}$, this being valid since the functional form of the cross-correlation coefficients (Eqn. 20) is symmetric in mode number. Finally, we have taken all of the $G_{m(n)}^{(3)}$'s to be constants, taking on their threshold values when the laser is above threshold. These coefficients depend on the carrier density, which becomes essentially clamped to its threshold value [29]-[30]. Any extra injected carrier density is quickly recombined in stimulated emission. There is, however, a slight increase of carrier density with injection current. According to Ohtsu [31], the fractional increase of carrier density to the fractional increase in injection current, i.e., $(n^{(0)}/n_{th}-1)/(J/J_{th}-1) = 1.7\times10^{-2}$.

We now turn our attention to the calculation of the total intensity noise. The integrals we need are obtained as follows:

$$\begin{aligned} Q &= \int_0^\infty dI_1 dI_2 e^{-U(I_1,I_2)} \\ &= \int_0^\infty dI_1 \exp\left[-\frac{1}{4}I_1^2+\frac{1}{2}a_1 I_1\right]\int_0^\infty dI_2 \exp\left[-\frac{1}{4}I_2^2-\frac{1}{2}(\xi I_1-a_2)I_2\right]. \end{aligned} \tag{27}$$

The integral over I_2 can be found as formula 3.462.1 in [33] (this formula will be used repeatedly):

$$\int_0^\infty x^{\nu-1}\exp[-\beta x^2-\gamma x]\,dx = \frac{\Gamma(\nu)}{(2\beta)^{\nu/2}}\exp\left(\frac{\gamma^2}{8\beta}\right)D_{-\nu}\left(\frac{\gamma}{\sqrt{2\beta}}\right), \tag{28}$$

where Γ is the gamma function and $D_{-\upsilon}$ is the parabolic cylinder function. We identify $\upsilon = 1$, $\beta = 1/4$ and $\gamma = \frac{1}{2}(\xi I_1 - a_2)$. Using formula 9.254.1 in [33] for D_{-1}, we obtain

$$Q = \int_0^\infty dI_1 \sqrt{\pi}\exp\left[\left(\frac{\xi I_1-a_2}{2}\right)^2+\frac{1}{2}a_1 I_1-\frac{1}{4}I_1^2\right]\mathrm{erfc}\left(\frac{\xi I_1-a_2}{2}\right), \tag{29}$$

where erfc is the error function complement defined by $\mathrm{erfc}(z) = \int_z^\infty \exp(-t^2)dt$. In a similar fashion, we obtain

$$\begin{aligned} \langle I_1^n\rangle = \frac{\sqrt{\pi}}{Q}\int_0^\infty dI_1\, I_1^n \exp\left[\frac{1}{4}(\xi^2-1)I_1^2+\frac{1}{2}(a_1-\xi a_2)I_1+\frac{1}{4}a_2^2\right] \\ \cdot\ \mathrm{erfc}\left[\frac{1}{2}(\xi I_1-a_2)\right]. \end{aligned} \tag{30}$$

$$\langle I_2^n \rangle = \frac{\sqrt{\pi}}{Q}\int_0^\infty dI_2\, I_1^n \exp\left[\frac{1}{4}(\xi^2-1)I_2^2+\frac{1}{4}(a_2-\xi a_1)I_2+\frac{1}{4}a_1^2\right] \cdot \mathrm{erfc}\left[\frac{1}{2}(\xi I_2-a_1)\right], \tag{31}$$

with n = 1,2. Finally, to get $\langle I_1 I_2 \rangle$, we must use $\upsilon = 2$. With the help of formula 9.254.2 of [33] for the parabolic cylinder function, we get

$$\langle I_1 I_2 \rangle = \frac{2}{Q}\int_0^\infty dI_1\, I_1 \exp\left[-\frac{1}{4}I_1^2+\frac{1}{2}a_1 I_1\right]\left\{1-\sqrt{\pi}\left[\frac{1}{2}(\xi I_1-a_2)\right] \cdot \exp\left(\frac{\xi I_1-a_2}{2}\right)^2 \mathrm{erfc}\left[\frac{1}{2}(\xi I_1-a_2)\right]\right\}. \tag{32}$$

The integrations in Eqns. 28-31 have to be done numerically, since there appear to be no expressions in closed form for these integrals. A fourth-order Runge-Kutta method [23] is used to carry out the integration for each value of injection current, using the analytical expressions for the pump parameters. To evaluate the error function complement, we use

$$\mathrm{erfc}(z) = \begin{cases} z^{-1}e^{-z^2}(0.5616-0.2103z^{-2}), & z>2, \\ 1-\mathrm{erf}(z), & 0\le z\le 2. \end{cases} \tag{33}$$

Here, erf(z) is the error function defined by $\mathrm{erf}(z) = \int_0^z \exp(-t^2)dt$. The first condition is obtained by noting from tables [34] that a graph of z $\exp(z^2)$ erfc(z) vs. z is very nearly a straight line. In the second condition, erf(z) is evaluated numerically using a ten-point Gauss-Legendre quadrature technique [23].

APPENDIX B

CALIBRATION OF SPECTROGRAPH DISPERSION

To determine the reciprocal dispersion of the grating spectrograph, light from a rubidium discharge lamp was focussed onto the entrance slit of the spectrograph. The spectrum of the lamp was imaged at the exit plane (actually an arc) of the spectrograph. The linear photodiode array was placed in the same plane. Its output showed the spectral distribution of the lamp (see Figure 20). The light intensity was so low that the photodiode array scan rate (see discussion below) had to be reduced to 10 Hz in order to accumulate enough charge in the diodes to give a reasonable signal. The oscilloscope was used in "average" mode to reduce the noise. As can be seen from the figure, the rubidium lines of 794.76 nm and

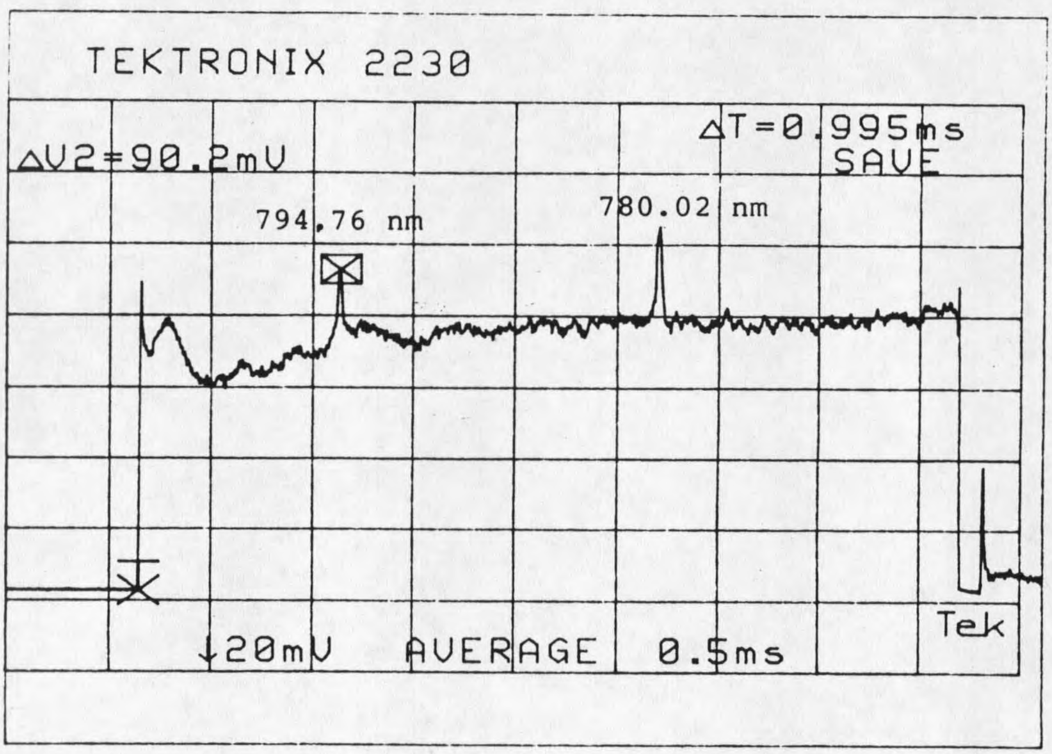

Figure 20. Spectrum of rubidium used to calibrate spectrograph reciprocal dispersion.

780.02 nm [35] stand out well enough from the background to be useful.

The photodiode array stores charge in each diode until read (discharged) by the controlling electronics. The amount of charge on a diode is proportional to the accumulated energy of the light incident on the diode and hence to the intensity. The diodes are read at a rate of approximately 4 microseconds per diode. Since the diodes are 25 microns apart, time can be converted to distance, which in turn can be converted to wavelength given the spatial position of known wavelengths. The electronics send the readout to the digital oscilloscope. The scope displays voltage (proportional to the light intensity) vs. time (proportional to wavelength), thus displaying the spectrum.

Determination of the reciprocal dispersion was carried out by finding the time difference between the two peaks, converting this value to a distance at the output plane, and then dividing the difference between the two wavelengths. With the observed time difference of 1.575 ms, the calculation went as follows:

$$\frac{(794.76\mathrm{nm}-780.02\mathrm{nm})}{1.575\mathrm{ms}}\frac{3.936\times10^{-3}\mathrm{ms}}{\mathrm{diode}}\frac{1\mathrm{diode}}{25\times10^{-3}\mathrm{mm}} = 1.48\frac{\mathrm{nm}}{\mathrm{mm}}. \qquad (34)$$

APPENDIX C

HIDDEN-LINE ALGORITHM FOR PLOTTING NOISE DATA

The "grand stability map" was produced by the computer using the following procedure: Each data pair of injection current and ac voltage in the file corresponding to the lowest case temperature was read and entered into a master map file. Each pair was stored in a variable which recorded the highest readings of ac voltage at a given current. Then each data pair of the next highest temperature file was read. An offset of 0.5 mV was added to the ac voltage. If this new value was larger than the high reading at that current, it was appended to the master file and also entered as the new high reading. If the offset value was not larger than the high reading, it was the high reading which was appended to the master file; the high reading was left unchanged. This allowed peaks to obscure flat regions.

The rationale behind this procedure was that slowly-varying trends in the data could be observed if the curves were presented offset from each other. If the offset was not great enough, the curves overlapped, causing visual confusion. The hidden-line procedure described above allowed many curves to be displayed on the same graph with little obscuration of important features.

APPENDIX D

DETERMINATION OF LINE OF CONSTANT JUNCTION TEMPERATURE

It was suspected that the "mountain ranges" lay along lines of constant junction temperature. It seemed reasonable that, because of joule heating, the junction temperature would rise with increased injection current even if the case temperature remained the same. The laser wavelength was used as an indicator of junction temperature constancy: If the junction temperature changed, the mode wavelength would also change. The following procedure was implemented: After consulting the stability map, a current-temperature combination was chosen for which the laser would operate in single mode. This formed the reference temperature of the junction. Now the task was to determine some other combinations which would yield the same junction temperature.

The spectrum was observed on the scope, note being taken of which diodes formed the peak and their relative heights. The centroid of the distribution was calculated in order to give a more precise estimate of the (relative) wavelength. This value became the reference wavelength: Any other case temperature-injection current pair which yielded the same wavelength corresponded to the same junction temperature.

After the case temperature was increased by a few tenths of a degree, the wavelength was recorded (again by calculating the centroid) and the current. The current was then decreased by increments, each time noting the wavelength. Using these data, it was determined at which current the wavelength had been the same as the reference wavelength. This current and the present case temperature had reproduced the reference junction temperature.

This procedure was repeated several times. The results are shown in Figure 17. As hypothesized, the points lay along a line which roughly paralleled the slope of the "mountain ranges". The line of best fit (by linear regression) has the equation $T_C = 37.53-0.311I$, where I is the current in milliamps and T_C is measured in degrees Celsius.

We note that a similar result has also been obtained by Yamada and Suematsu [24], who looked at temperature compensation as a means of mode stabilization. They found that they could keep the wavelength constant by changing the case temperature by -0.11°C per milliamp of injection current. Our value was -0.31°C/ma, the difference likely being due to different thermal masses, heat conduction paths and different leakage currents, which contribute to joule heating. Not all injected current necessarily passes through the active region; that which does not is called leakage current.

APPENDIX E

DETERMINATION OF JUNCTION TEMPERATURE

An analysis of the heat flow in the laser and its immediate surroundings was performed to determine whether the junction temperature could be measured with techniques at hand (as compared to pulsed methods [20]). As shown below (see Figure 21), heat flows occur between the junction, the aluminum plate and the surroundings. The flow is assumed to be conductive between the junction and plate and between the plate and the surroundings (via thermoelectric modules); it is assumed that radiation is the heat flow mechanism between the surroundings and the junction, as the latter is not in physical contact with the surroundings. The injection current is assumed to be a source of heat. Four heat flow equations can be written as follows:

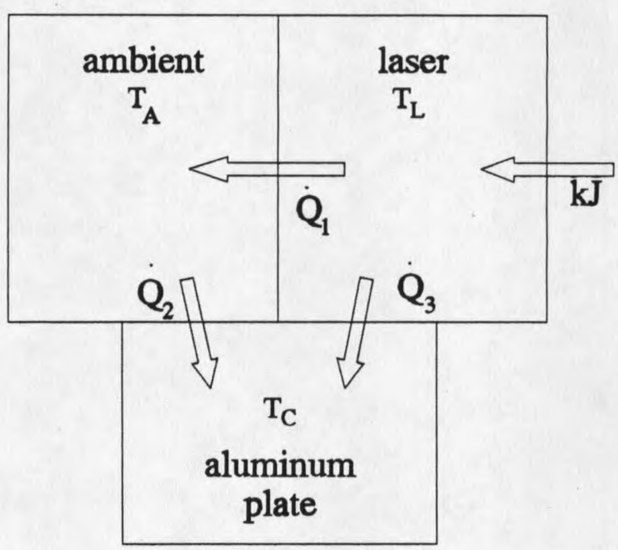

Figure 21. Heat flow schematic. The dQ/dt's are heat flow rates, while kJ represents joule heating.

$$
\begin{aligned}
\frac{dQ_1}{dt} &= c_1(T_L - T_A),\\
\frac{dQ_2}{dt} &= c_2(T_A - T_C),\\
\frac{dQ_3}{dt} &= c_3(T_L - T_C),\\
kI &= \frac{dQ_1}{dt} + \frac{dQ_3}{dt},
\end{aligned}
\tag{35}
$$

where c_1, c_2, c_3 and k are constants of proportionality determined by coefficients of thermal conductivity, emissivity and geometrical factors; T_L, T_A and T_C are the junction, ambient (surroundings) and case temperatures in °C, respectively. The dQ/dt's and kJ are heat flow rates as defined in Figure 21, J being the injection current.

It should be noted that equations involving heat flow to and from the surroundings use a simple temperature difference rather than differences of T^4, as one might expect for radiative transfer of energy. One can write, for example, the following equations for the heat flow rate between the laser and the surroundings:

$$
\begin{aligned}
\frac{dQ_1}{dt} &= c'(T_L^4 - T_A^4)\\
&= c'(T_L^2 + T_A^2)(T_L^2 - T_A^2)\\
&= c'(T_L^2 + T_A^2)(T_L + T_A)(T_L - T_A)\\
&= c(T_L - T_A),
\end{aligned}
\tag{36}
$$

where c is approximately constant for the range of temperatures encountered. The heat flow rate can therefore be approximated as stated.

If we solve these equations for the case temperature T_C at equilibrium, we obtain:

$$T_C = aT_L - bT_A - cI, \tag{37}$$

where $a = (c_1+c_3)/c_3$, $b = c_1/c_3$ and $c = k/c_3$.

Equation 36 gives the case temperature in terms of the junction and ambient temperatures and the injection current. Later, of course, we will invert the equation to get the junction temperature in terms of the other quantities. For now, we note that the experimentally measurable (and controllable) parameters are the ambient temperature, the case temperature and the injection current. Now, k has already been determined: It is the coefficient of the injection current in the equation of the line of constant junction temperature as described in Appendix C. All that remains, then, is to find either a or b in Eqn. 36, since, by their definitions, a = b+1. Taking small differences in Eqn. 36 while holding T_L and T_C constant, we obtain:

$$b = -c\frac{\Delta I}{\Delta T_A}, \tag{38}$$

where ΔI and ΔT_A are changes in the injection current and the ambient temperature, respectively. The experimentally obtained value were $\Delta I = 0.4$ ma and $\Delta T_A = -5.0°C$, giving values of b = 0.025 and a = 1.025. Thus, Eqn. 36 can b written explicitly as

$$T_C = 1.025T_L - 0.025T_A - 0.311I, \tag{39}$$

or inverted to give, as advertised,

$$T_L = 0.976T_C + 0.024T_A + 0.303I \tag{40}$$

From this we can see that the ambient temperature, at least in the present temperature-controlled setup, has a small effect on the junction temperature. This was born out by making a stability map of a selected portion of the current-temperature plane at a different ambient temperature. This map was slightly shifted from the original, but was otherwise essentially the same.

Of greatest importance is the case temperature, followed by the heating effect of the injection current. The fact that the injection current can cause a significant temperature change in the junction is an effect of which little account is taken in the literature. Exceptions exist [16],[24],[26],[31],[36].

APPENDIX F

MEASUREMENT OF RATE OF CHANGE OF MODE AND GAIN PEAK WAVELENGTHS WITH TEMPERATURE

To measure how rapidly the wavelengths of the modes and the gain peak change with case temperature with the output power held constant, it was only necessary to implement a variation of the procedure outlined in Appendix D. The centroid of the mode wavelength was noted at each of several case temperatures. Each time the laser switched modes, a similar set of measurements was carried out. The result was the series of steps seen in Figure 4. The average of the slopes of the line segments was 0.065 nm/°C. The gain peak's rate of change with case temperature was found by taking the slope of the line connecting the centers of the line segments, the assumption being that the gain peak is centered over a longitudinal mode between mode hops. The gain peak shift rate was found to be 0.208 nm/°C. These values are in good agreement with Wieman [3].

APPENDIX G

THEORETICAL CALCULATION OF AC VOLTAGE

The noise spectrum is taken to be a Lorentzian centered at the origin. We write

$$S(f) = \frac{S(0)}{1+(f/f_c)^2}, \tag{41}$$

where f is the frequency, S(f) is the noise spectrum, and f_c, called the cutoff frequency, is the half-width defined by $S(f_c) = S(0)/2$. Setting the total noise equal to the integral of S(f) over all (positive) frequencies, we obtain

$$\begin{aligned} \langle(\Delta I)^2\rangle^{1/2} &= \int_0^\infty \frac{S(0)\,df}{1+(f/f_c)^2} \\ &= \frac{\pi}{2} S(0) f_c . \end{aligned} \tag{42}$$

The ac voltage depends on the detection system response convolved with the noise spectrum. If g(f) is the system response function, we have

$$vac = \int_0^\infty g(f)\,S(f)\,df, \tag{43}$$

where vac is the (unnormalized) ac voltage. For simplicity, we take the system response to be flat from zero frequency to a frequency f_d, vanishing otherwise. With g(f) = 1 when $0 \leq f \leq f_d$, and g(f) = 0 when $f \geq f_d$, we have

$$\begin{aligned} vac &= \int_0^\infty g(f)\,S(f)\,df \\ &= \int_0^{f_d} S(f)\,df \\ &= \frac{2}{\pi}\langle(\Delta I)^2\rangle^{\frac{1}{2}} \tan^{-1}\left(\frac{f_d}{f_c}\right). \end{aligned} \tag{44}$$

A functional form of Ohtsu's graph [12] of f_c vs $\langle I_1\rangle/\langle I_2\rangle$, obtained by trial and error, is given by

$$f_c = 50\ \text{kHz} + 500\ \text{kHz}\ \ln(I_>/I_<), \qquad (45)$$

where $I_>$ ($I_<$) is the greater (lesser) of the two intensities (see Figure 22). This (expression for f_c is used in Eqn. 44 to obtain Figure 16.

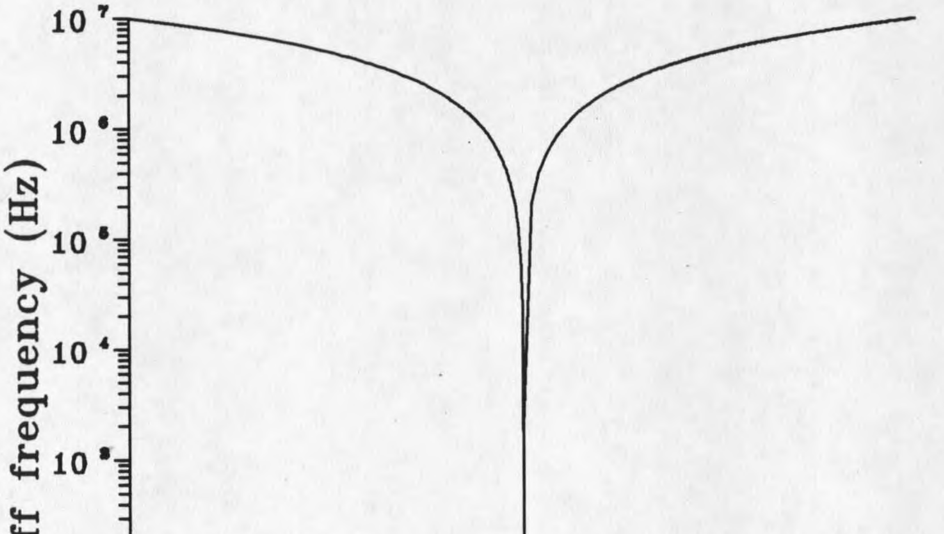

Figure 22. Plot of cutoff frequency vs. ratio of average intensities.

LITERATURE CITED

LITERATURE CITED

1. Motoichi Ohtsu, Hiromasa Suzuki, Koukichi Nemoto and Yasuaki Teramachi, "Narrow-linewidth tunable visible InGaAlP laser, application to spectral measurements of lithium, and power amplification," Japanese Journal of Applied Physics **29**, L1463-L1465 (July 1966).

2. Wayne Lo and Richard F. Majkowski, "Detection of oxygen concentration in silicon wafers using a tunable diode laser," IEEE Journal of Quantum Electronics **QE-21**, 395-399 (April 1985).

3. Carl E. Wieman and Leo Hollberg, "Using diode lasers for atomic physics," Review of Scientific Instruments **62**,1-19 (January, 1991).

4. Yoshihisa Yamamoto, Susumu Machida, Wayne H. Richardson, "Photon number squeezed states in semiconductor lasers," Science **255**, 1219-1224 (1992).

5. Edward C. Gage and Brian J. Bartholomeusz, "Directional asymmetries due to write-laser mode hopping during optical recording," Journal of Applied Physics **69**, 569-573 (15 January 1991).

6. T. Gotoh, A. Arimoto, M. Ojima and N. Chinone, " Characteristics of laser diodes and picture quality," Proceedings of SPIE, Vol. 329, Issue on Optical Disk Technology, 56-60 (1982).

7. Ken-ichi Sato, "Intensity noise of semiconductor laser diodes in fiber optic analog video transmission," IEEE Journal of Quantum Electronics **QE-19**, 1380-1391 (September, 1983).

8. Richard A. Linke, Bryon L. Kasper, Charles A. Burrus, Jr., Ivan P. Kaminow, J.-S. Ko, and Tien Pei Lee, " Mode power partition events in nearly single-frequency lasers," Journal of Lightwave Technology LT-3,706-711 (June, 1985).

9. Robert H. Wentworth, George E. Bodeep and Thomas E. Darcie, "Laser mode partition noise in lightwave systems using dispersive optical fiber," Journal of Lightwave Technology **10**, 84-88 (1992).

10. Stewart E. Miller, "On the injection laser contribution to mode partition noise in fiber telecommunications systems," IEEE Journal of Quantum Electronics **25**, 1771-1781 (1986).

11. George R. Gray and Rajarshi Roy, "Bistability and mode hopping in a semiconductor laser," Journal of the Optical Society of America B **8**, 632-638 (March, 1991).

12. Motoichi Ohtsu and Yasuaki Teramachi, "Analyses of mode partition and mode hopping in semiconductor lasers," IEEE Journal of Quantum Electronics **25**, 31-38 (1989)

13. R.W. Tkach and A.R. Chraplyvy, "Regimes of feedback effects in 1.5-μ distributed feedback lasers," Journal of Lightwave Technology **LT-4**, 1655-1661 (November, 1986).

14. Nagaatsu Ogasawara, Ryoichi Ito, Masahiro Kato and Yoshitaba Takahashi, "Mode switching in injection lasers induced by temperature variation and optical feedback," Japanese Journal of Applied Physics pt.1 **22**, 1684-1690 (1983).

15. Minoru Yamada, "Transverse and longitudinal mode control in semiconductor injection lasers," IEEE Journal of Quantum Electronics **QE-19**, 1365-1379 (1983).

16. M. M-Tehrani and L. Mandel, "Coherence theory of the ring laser," Physical Review A **17**, 677-693 (1978).

17. Govind P. Agrawal, "Mode partition noise and intensity correlation in a two-mode semiconductor laser," Physical Review A **37**, 2488-2494 (1988).

18. Melvin Lax, "Classical Noise IV: Langevin methods," Reviews of Modern Physics **38**,541-566 (1966).

19. Motoichi Ohysu, Yasuaki Teramachi, Yoshihiro Otsuka and Akio Osaki, "Analyses of mode-hopping phenomena in an AlGaAs laser," IEEE Journal of Quantum Electronics **QE-22**, 535-543 (1986).

20. Wlodzimierz Nakwaski, "An exact method of measuring the junction temperature in GaAs laser diodes," Electron Technology **11**, 37-55 (1978).

21. Sadao Adachi, "GaAs, AlAs and $Al_xGa_{1-x}As$: Material parameters for use in research and device applications," Journal of Applied Physics **58**, R1-R29 (1985).

22. M. Sargent III, M.O. Scully and W.E. Lamb, Jr., *Laser Physics*. Reading, MA: Addison-Weseley, 1974, ch. 9.

23. Julien C. Sprott, Ed., *Numerical Recipes: Routines and Examples in BASIC*. New York, Cambridge University Press, 1991.

24. Minoru Yamada and Yasuharu Suematsu, "A condition of single longitudinal mode operation in injection lasers with index-guiding structure," IEEE Journal of Quantum Electronics **QE-15**, 743-749 (1979).

25. David Chambliss and Mark Johnson, "Structure-dependent wavelength shifts in AlGaAs lasers near threshold, and their application to a wavelength-stable source," Optics Communications, **48**, 343-346 (1984).

26. Tien-Pei Lee, Charles A. Burrus, John A. Copeland, Andrew G. Dentai and Dietrich Marcuse, "Short-cavity InGaAsP injection lasers: Dependence of mode spectra and single-longitudinal-mode power on cavity length," IEEE Journal of Quantum Electronics **QE-18**, 1101-1112 (1982).

27. S.M. Sze, *Physics of Semiconductor Devices*. New York: Wiley-Interscience, 1981), ch. 13.

28. X.W. Wang, D.L. Lin and F.T.Hioe, "Mean switching time of bistable two-mode lasers," Physical Review A **34**, 1251-1259 (1986).

29. J.C. Camparo, "The diode laser in atomic physics," Contemporary Physics **26**, 443-476 (1985).

30. G.P. Agrawal and N.K. Dutta, *Long-Wavelength Semiconductor Lasers*. New York: Van Nostrand Reinhold, 1986, p. 230.

31. Motoichi Ohtsu, Yasuaki Teramachi and Tetsuya Miyazaki, "Mode stability analysis of nearly single-longitudinal-mode semiconductor lasers," IEEE Journal of Quantum Electronics 24, 716-723 (1988).

32. M. Ohtsu, Y. Otsuka and Y. Teramachi, "Precise measurements and computer simulations of mode-hopping phenonema in semiconductor lasers," Applied Physics Letters **46**, 108-110 (1985).

33. I.S. Gradshteyn and I.M. Ryzhik, Ed., *Table of Integrals, Series* and Products. Florida: Academic Press, 1980.

34. Milton Abramowitz and Irene A. Stegun, Ed., *Handbook of Mathematical Functions*. New York: Dover Publications, Inc, 1965, p. 316.

35. Robert C. Weast, Ed., *Handbook of Chemistry and Physics*, 55th edition. Ohio: CRC Press, 1974, p. E-214.

36. Naoki Chinone, Takao Kuroda, Tsukuru Ohtoshi, Takeo Takahashi and Takashi Kajimura, "Mode-hopping noise in index-guided semiconductor lasers and its reduction by saturable absorbers," IEEE Journal of Quantum Electronics QE-21, 1264-1269 (August, 1985).